Repurposing celecoxib for colorectal cancer targeting via pH-triggered ultra-elastic nanovesicles: Pronounced efficacy through up-regulation of Wnt/β-catenin pathway in DMH-induced tumorigenesis

Shahira F. El Menshawe [a], Khaled Shalaby [b,*], Mohammed H. Elkomy [b], Heba M. Aboud [a,*], Yasmin M. Ahmed [c], Abdelmeged A. Abdelmeged [d], Marwa Elkarmalawy [e], Mahmoud A. Abou Alazayem [d], Amani M. El Sisi [a]

[a] Department of Pharmaceutics and Industrial Pharmacy, Faculty of Pharmacy, Beni-Suef University, Beni-Suef, Egypt
[b] Department of Pharmaceutics, College of Pharmacy, Jouf University, Sakaka, Saudi Arabia
[c] Department of Pharmacology and Toxicology, Faculty of Pharmacy, Nahda University, Beni-Suef, Egypt
[d] Department of Pharmaceutics, Faculty of Pharmacy, Nahda University, Beni-Suef, Egypt
[e] Department of Pharmaceutics and Drug Manufacturing, Faculty of Pharmacy, Modern University for Technology and Information, Cairo, Egypt

ARTICLE INFO

ABSTRACT

Celecoxib (CLX), a selective inhibitor for cyclooxygenase 2 (COX-2), has manifested potential activity against diverse types of cancer. However, low bioavailability and cardiovascular side effects remain the major challenges that limit its exploitation. In this work, we developed ultra-elastic nanovesicles (UENVs) with pH-triggered surface charge reversal traits that could efficiently deliver CLX to colorectal segments for snowballed tumor targeting. CLX-UENVs were fabricated via a thin-film hydration approach. The impact of formulation factors (Span 80, Tween 80, and sonication time) on the nanovesicular features was evaluated using Box–Behnken design, and the optimal formulation was computed. The optimum formulation was positively coated with polyethyleneimine (CLX-PEI-UENVs) and then coated with Eudragit S100 (CLX-ES-PEI-UENVs). The activity of the optimized nano-cargo was explored in 1,2-dimethylhydrazine-induced colorectal cancer in Wistar rats. Levels of COX-2, Wnt-2 and β-catenin were assessed in rats' colon. The diameter of the optimized CLX-ES-PEI-UENVs formulation was 253.62 nm, with a zeta potential of −23.24 mV, 85.64% entrapment, and 87.20% cumulative release (24 h). ES coating hindered the rapid release of CLX under acidic milieu (stomach and early small intestine) and showed extended release in the colon section. In colonic environments, the ES coating layer was removed due to high pH, and the charge on the nanovesicular corona was shifted from negative to positive. Besides, a pharmacokinetics study revealed that CLX-ES-PEI-UENVs had superior oral bioavailability by 2.13-fold compared with CLX suspension. Collectively, these findings implied that CLX-ES-PEI-UENVs could be a promising colorectal-targeted nanoplatform for effective tumor management through up-regulation of the Wnt/β-catenin pathway.

1. Introduction

Colorectal cancer (CRC) remains a challenging ailment despite substantial treatment and early diagnosis breakthroughs, with poor overall survival rates over the long term (Buzzelli et al., 2018). CRC is the second most common cause of cancer-related deaths globally (Srivastava et al., 2021). Smoking and diet (containing aromatic and heterocyclic amines) are prime risk factors for CRC (Venkatesan et al., 2011).

Chemotherapy is the most important therapeutic option; nevertheless, its long-term drug resistance offers considerable challenges (Srivastava et al., 2021). In addition, the significant chemotherapeutic-related side effects might be deadly in certain cases. Therefore, the key to effectively treating this fatal disease is using therapeutic approaches with low or no toxicities. As a result, there is an imperious need for novel medications that can effectually treat CRC. Intriguingly, the approval of non-cancer drugs has become a crucial strategy for accomplishing effective cancer

therapies as a result of rapid drug development and reduced costs, as information on pharmacokinetics, safety profiles, mechanisms of action, and formulations is already available to aid their clinical applications (Hatem et al., 2019; Pushpakom et al., 2019).

Evidence from numerous lines of research shows that CRC and adenomatous polyps have higher cyclooxygenase-2 (COX-2) as well as prostaglandin E2 levels (Wang and DuBois, 2006). Various cell culture, animal, and epidemiological investigations have established the anti-tumorigenic potential of celecoxib (CLX), accomplished by selective COX-2 inhibition (Arber et al., 2006). In preclinical investigations, CLX has shown significant anticancer effects against lung, colorectal, and breast cancer (Hsiao et al., 2007; Bijman et al., 2008). Consequently, the FDA authorized CLX for the adjuvant therapy of individuals with CRC (Steinbach et al., 2000; Kuwai et al., 2008). Actually, the expression of COX-2 is activated by several mediators, including the Wnt/β-catenin pathway, contrary to COX-1, which is constitutively synthesized in the tissues. Wnt proteins are a cluster of secreted ligands that regulate essential cellular functions, such as determining cell fates, cellular proliferation rates, survival, differentiation, and adhesion levels (Zhao et al., 2022). The attachment of Wnt to its primary receptor stimulates its signaling attracting the cytosolic protein (Kolluri and Ho, 2019) and interrupting the development of the axin/glycogen synthase kinase 3 (GSK3)/adenomatous polyposis coli (APC) complex and enhancing the cytoplasmic accumulation of catenin (Terry et al., 2006), then translocating into the nucleus and interacting with T cell factor/lymph enhancer factor 1 (TCF/LEF1) to activate the production of Wnt-targeted genes (Gehrke et al., 2009; Aoki et al., 2022). Similarly, the stromal cell-derived factor 1/C-X-C motif chemokine receptor 4 (SDF-1/CXCR4) axis signaling pathway is clinically significant for the metastasis and spread of colorectal cancer (Kim et al., 2006; Wang et al., 2010). To our knowledge, this work is the first to establish that invasiveness and metastasis prevention in CRC occur through Wnt/β-catenin/TCF1/LEF1-mediated inhibition of COX-2. We hypothesized that inhibition of COX-2 activity will decrease chemoresistance in CRC, suggesting a central function for this system in such disease.

Despite the efficacy of CLX in CRC treatment, adverse effects, including thrombosis and cardiovascular risk, have limited its use in cancer chemotherapy (Auman et al., 2008; Srivastava et al., 2021). To diminish the potential risk, it was recommended to use CLX for the shortest feasible period at the lowest effective dosage. In addition, CLX has limited water solubility and a narrow therapeutic index, making it challenging to formulate with conventional dosage forms for the treatment of CRC (Venkatesan et al., 2011). Furthermore, the therapeutic dose of CLX in the tumor tissue was reported to be declined due to its rapid plasma elimination (Paulson et al., 2000). In addition, dimethyl sulfoxide (DMSO) is often used as a solvent for CLX during in vitro studies, which is inappropriate for usage in vivo (Hsiao et al., 2007; Sasaki et al., 2007; Bijman et al., 2008). Consequently, it is essential to identify a particular cancer cell-targeted drug delivery system (DDS) for CLX administration.

The potency of an anticancer drug and the use of an efficient DDS determine its efficacy in cancer patients. Thus, anticancer-targeted delivery to the tumor site by modifying the biodistribution and pharmacokinetic features of DDS is a current focus of cancer therapy (Lu et al., 2008; Hiremath et al., 2009). For cancer treatment, numerous DDS, including polymeric micelles, parenteral emulsions, nanoparticles, and liposomes, have been explored (Mandal and Kundu, 2009; Qu et al., 2009; Kundu et al., 2010). Among these approaches, nanovesicular-mediated transport offers several benefits, including a small diameter, less toxicity, improved drug stability and solubility, greater medication effectiveness, and the capacity to attain steady-state therapeutic levels over a longer period (He et al., 2009).

Among the promising nano-cargos for colon drug delivery, spanlastic systems (novel ultra-elastic nanovesicles, UENVs) can be deemed as an optimum approach. UENVs are surfactant-based colloidal drug carriers with spheroid structures consisting of amphiphilic substances (Tayel et al., 2015). These elastic cargos are constructed of Span 80 (surfactant) and Tween 80 as edge activator and exhibit great elasticity and deformability due to the organization of surfactant macromolecules as a bilayer membrane completely enclosing an aqueous solute solution. Other hydrophilic surfactant substances increase the flexibility of lipid bilayers in spanlastic systems by creating pores and disrupting the membranes (Tayel et al., 2015). During formulation, sorbitan-tailored vesicles with flexible walls are produced by modifying traditional niosomes with EA amalgamation. EA provides elasticity by destabilizing vesicles and fluidizing their bilayers by decreasing interfacial tension (El Menshawe et al., 2019).

The main obstacle to colon-targeted drug delivery is premature medication release in acidic environments (stomach and early small intestine) (Naeem et al., 2018). The surface features of nano-cargos have been shown to substantially affect their selective accumulation inside cancer cells. According to a previous study, the cationic feature of DDS may facilitate mucoadhesion to CRC tissues and absorption by tumor cells (Naeem et al., 2018). Therefore, using polyelectrolyte complexes in synthesizing cationic UENVs could improve mucoadhesion, cellular absorption, and acidic stability. The use of positively charged polyethyleneimine (PEI) assists in accumulating UENVs in tissues due to interaction with negatively charged biological molecules (Naeem et al., 2018). In acidic environments, the cationic polymer coating may be incapable of preventing drug leakage. The Eudragit S100 (ES) coating can resolve the issue of undesired rapid release in acidic conditions and exhibit extended drug release in the colon. Therefore, coating the cationic UENVs with a pH-sensitive polymer such as ES could delay medication release in the gastrointestinal tract (GIT). The layer would disintegrate at a pH of 7.4 in the colon, exposing the cationic surface of UENVs and promoting their adsorption in malignant colon cells (Naeem et al., 2018). Hence, the proposed ES-PEI-UENVs could potentiate CLX bioavailability and protect against colon cancer.

Thus, in the current work, we formulated UENVs containing CLX (CLX-UENVs) by combining Span 80 and Tween 80 to be assessed as a possible therapy for colon cancer. The impact of formulation parameters (Span 80, Tween 80, and sonication time) on UENVs features was assessed using the Box-Behnken design, and the optimal formulation was estimated. The optimized CLX-UENVs formulation was positively coated with PEI (CLX-PEI-UENVs) and then coated with ES 100 (CLX-ES-PEI-UENVs). The designed CLX-ES-PEI-UENVs were evaluated physiochemically to determine their suitability for colon administration. The pharmacokinetics of CLX after oral administration of CLX-ES-PEI-UENVs and an aqueous CLX suspension in rats were assessed to investigate the efficacy of the developed systems. Furthermore, the underlying molecular mechanism for the antitumor activity of CLX on 1,2-dimethylhydrazine (DMH)-induced CRC in rats was explored.

2. Materials and methods

2.1. Materials

Celecoxib was supplied from SEDICO Pharmaceutical Company (Cairo, Egypt). Polyethyleneimine, Span 80, Eudragit S100, sodium carboxymethyl cellulose (MW: 90000 Da), 1,2-dimethylhydrazine, methanol (HPLC grade), Tween 80, and chloroform (HPLC grade) were purchased from Sigma-Aldrich (St. Louis, MO). Dialysis membrane (MW cut off: 12000 Da) was purchased from SERVA Electrophoresis GmbH (Heidelberg, Germany). Enzyme-linked immunosorbent assay (ELISA) kits for cyclooxygenase-2 (Catalog no. MBS266603) and Wnt-2 (Catalog no. MBS7700340) were procured from MyBioSource (San Diego, CA, USA) while that for β-catenin (Catalog number K3383–100) was obtained from BioVision (Waltham, MA, USA). Monoclonal antibody for CXCR-4 (Catalog no. PA1–21626) for immunohistochemistry assay and primers for TCF3 (Catalog no. PA5–20900) and LEF1 (Catalog no. PA5102851) for qRT-PCR were purchased from ThermoFisher (Inchinnan Business Park, Paisley, UK). Other ingredients and solvents

utilized were of analytical grade.

2.2. Design and optimization of experiments

Box-Behnken design is utilized for the generation of higher-order response surfaces, adopting lesser needed runs than a full factorial designing. It employed 12 middle edge nodes and three center nodes to fit a second-order equation (Ahmad et al., 2020). Such design was used to study the independent variables effects on CLX-UENVs features using Design Expert® software (12.0.3.0, Stat-Ease Inc., USA). Preliminary experiments (data not presented) were conducted to establish the probable independent variable ranges, which guided the choice of factors and the used levels. Span 80 amount ranged from 160 to 200 mg, Tween 80 amount ranged from 10 to 30% (w/w %), and sonication time ranged from 0 to 10 min, were the independent variables. Vesicle size (VS), zeta potential (ZP), entrapment efficiency (EE), and cumulative drug release after 24 h (CR) were the dependent variables. Fifteen experimental runs (12 formulations and three repeated central points) were conducted, as shown in Table 1. Using the R plot3D package, 3D surface graphs were generated (Panda et al., 2021). The optimization was based on a minimum VS and a maximum ZP, EE, and CR to get the formulation with the highest desirability (Salem et al., 2022). Table 1 lists the independent variable levels and the experimental runs produced by the Box-Behnken design.

2.3. Preparation of CLX-UENVs

CLX-UENVs were assembled via the thin film hydration procedure (El Menshawe et al., 2019). In this procedure, Span 80 and CLX (10 mg) were added to a round-bottom flask and dissolved by a chloroform-methanol combination (2:1). The organic solvent was then evaporated at 55 °C using a rotary evaporator (Heidolph Laborota 4000 Series, Heizbad, Germany) at 100 rpm, creating a thin film on the flask wall. By flask rotation in a water bath at 55 °C and normal pressure for 30 min, the film was hydrated with phosphate-buffered saline (PBS, 10 mL, pH 7.4) containing Tween 80. As seen in Table 1, the resultant dispersion was then sonicated (Sonix TV ss-series, North Charleston, SC, USA). The formed dispersions were stored in a refrigerator (4 °C) overnight to allow them to mature, and then they were used for further experiments.

2.4. CLX-UENVs characterization and optimization

2.4.1. Vesicle size (VS) and zeta potential (ZP) analysis

The mean CLX-UENVs diameter and polydispersity index (PDI) were assessed by the dynamic light scattering (DLS) technique in the Zetasizer Nano ZS (Malvern Instruments, UK) (Aboud et al., 2018). Before analysis, the CLX-UENVs dispersion was diluted with purified water (1:10), and the assessment was performed at room temperature (El Menshawe et al., 2019). The ZP of CLX-UENVs (surface charge) was assessed via a laser doppler micro-electrophoresis approach in Zetasizer Nano ZS.

2.4.2. Measurement of entrapment efficiency

The EE of CLX in CLX-UENVs was determined by analyzing CLX in the supernatant and then deducting it from the amount added during formulation (10 mg). The supernatant containing free CLX was separated using a cooling centrifuge (SIGMA 3-30 K, Germany) at 4 °C (14,000 rpm, 2 h) (Khallaf et al., 2020). The resultant supernatant was then separated using a nylon syringe filter (0.45 μm). After appropriate dilution, the CLX concentration was estimated using a spectrophotometer (Shimadzu UV-1800, Tokyo, Japan) at 252 nm. The encapsulation efficiency of CLX inside CLX-UENVs was estimated using the following formula:

$$EE\% = \frac{Total\ amount\ of\ CLX - free\ CLX}{Total\ amount\ of\ CLX} \times 100$$

Table 1
Independent variables, experimental runs, and response variables for the formulations of CLX-UENVs according to the Box Behnken design.

Independent factors								Levels
					-1	0		1
X_1: Span 80 (mg)					160	180		200
X_2: Tween 80 (w/w %)					10	20		30
X_3: Sonication time (min)					0	5		10

Run	X_1	X_3	X_2	VS (nm)	ZP (mV)	EE (%)	CR (%)	PDI[¥]
R1	160	10	5	267.81 ± 2.96	−8.66 ± 0.18	50.03 ± 3.21	38.26 ± 5.06	0.157 ± 0.023
R2	160	20	0	264.43 ± 13.05	−7.79 ± 0.68	68.62 ± 2.57	43.20 ± 3.64	0.457 ± 0.026
R3	160	20	10	232.17 ± 17.04	−8.39 ± 0.49	60.21 ± 2.05	45.46 ± 3.89	0.086 ± 0.012
R4	160	30	5	227.62 ± 10.47	−5.02 ± 0.20	58.26 ± 2.12	46.96 ± 3.26	0.115 ± 0.016
R5	180	10	0	219.18 ± 7.15	−12.91 ± 0.13	83.48 ± 1.91	48.84 ± 4.13	0.142 ± 0.034
R6	180	10	10	217.74 ± 14.65	−12.09 ± 0.40	76.67 ± 3.32	49.59 ± 3.24	0.397 ± 0.016
R7*	180	20	5	217.63 ± 4.12	−11.85 ± 0.44	84.72 ± 2.73	59.36 ± 4.23	0.268 ± 0.021
R8*	180	20	5	213.86 ± 9.64	−11.66 ± 0.47	85.35 ± 2.93	60.11 ± 2.93	0.214 ± 0.028
R9*	180	20	5	199.63 ± 9.45	−10.43 ± 1.33	86.54 ± 1.97	62.74 ± 3.74	0.168 ± 0.019
R10	180	30	0	195.35 ± 18.77	−9.51 ± 1.31	84.86 ± 2.04	63.86 ± 4.42	0.135 ± 0.023
R11	180	30	10	185.13 ± 26.70	−9.09 ± 1.10	84.53 ± 3.39	67.62 ± 3.26	0.147 ± 0.015
R12	200	10	5	180.18 ± 25.25	−13.83 ± 0.47	86.75 ± 2.72	72.88 ± 3.77	0.290 ± 0.026
R13	200	20	0	179.91 ± 24.16	−13.06 ± 0.56	93.07 ± 2.57	82.65 ± 2.707	0.201 ± 0.026
R14	200	20	10	152.76 ± 15.33	−13.27 ± 0.17	91.46 ± 2.29	90.16 ± 3.82	0.275 ± 0.023
R15	200	30	5	129.53 ± 10.85	−12.81 ± 0.13	87.91 ± 2.51	93.92 ± 4.19	0.069 ± 0.033

Data are mean values ($n = 3$) ± SD.
* Indicates the center point of the design.
¥ Excluded from optimization.

2.4.3. Cumulative release (CR)

The CLX release from CLX-UENVs was determined in vitro by vertical Franz cells (5 cm²) (Elkomy et al., 2022b). The release medium was employed with pH values that gradually changed from 1.2 (acidic buffer, 2 h) to 6.8 (PBS, 6 h) and to 7.4 (PBS, 24 h), respectively, to represent the stomach, upper small intestine and ileum, and colon (Vandamme et al., 2002). A certain quantity of various CLX-UENVs formulations (3 mg of CLX in each) was added to the donor chamber. Seventy mL of the release medium containing Tween 80 (0.1% w/v) were introduced to the receptor chamber. The experiments were conducted at a temperature of 37 °C and a stirring speed of 100 rpm. At predefined intervals, aliquots (3 mL) were collected from the receptor chamber and replaced with an equivalent fresh receptor medium. The

obtained aliquots were diluted, filtered, and subjected to spectrophotometric analysis at 252 nm. The cumulative release (CR) results after 24 h were used in the optimization process.

2.5. Formulation of CLX-ES-PEI-UENVs

The CLX-PEI-UENVs were fabricated by adding PEI (0.25%) to PBS containing Tween 80, and the same approach described above was followed. Furthermore, CLX-ES-PEI-UENVs were prepared by incubating CLX-PEI-UENVs with moderate shaking for 1 h in an anionic solution of ES in PBS at a core-to-coat ratio of 1:4 (Al-Mahallawi et al., 2017; Naeem et al., 2018).

2.6. Characterization of CLX-ES-PEI-UENVs

2.6.1. VS, PDI, ZP, and EE analysis

As previously outlined, the VS, PDI, and ZP of CLX-ES-PEI-UENVs were assessed. In addition, the EE of CLX inside CLX-ES-PEI-UENVs was estimated.

2.6.2. Morphological evaluation

The morphology of CLX-UENVs, CLX-PEI-UENVs, and CLX-ES-PEI-UENVs was assessed via a transmission electron microscope (JEM-1400, Jeol, Tokyo, Japan). On a carbon-coated copper grid, one droplet of the optimized formulation after dilution (1:10) was placed, allowed to dry, and then stained with an aqueous solution of phosphotungstic acid (2%) as a negative stain. Finally, it is analyzed using a TEM with an 80 kV (Salem et al., 2022).

2.6.3. pH-dependent in vitro drug release and ZP

As described before, vertical Franz cells were used to perform in vitro release tests of CLX from CLX-UENVs, CLX-PEI-UENVs, and CLX-ES-PEI-UENVs. The surface charge of CLX-ES-PEI-UENVs was measured by incubating the dispersion in buffer solutions with varying pH levels (1.2, 6.8, or 7.4) for a predetermined period while being shaken in a water bath at 60 rpm and 37 °C. Next, the resulting dispersion was centrifuged and redistributed in distilled water. As mentioned before, the ZP of CLX-ES-PEI-UENVs was evaluated using a Zetasizer Nano-ZS.

2.6.4. Short-term stability

The stability study of the optimal CLX-ES-PEI-UENVs formulation was performed by keeping it in a glass vial in the refrigerator (4 °C). After 0, 1, 2, and 3 months, samples were drawn from the glass vial and analyzed for mean VS, EE, and ZP. In addition, the physical appearance was evaluated for aggregation, separation, or precipitation.

2.7. In vivo pharmacokinetic studies

2.7.1. CLX administration to rats

The pharmacokinetics of the orally administered CLX-ES-PEI-UENVs were compared with those of the orally administered conventional CLX suspension (CLX-SUSP). Following approval from the Local Institutional Animal Ethics Committee at Beni-Suef University (Acceptance no: 022–292), twelve male Wistar rats (200–250 g), procured from the animal facility of Nahda University (Beni-Suef, Egypt), were utilized in this study. The procedures were conducted in accordance with the Guide for the Care and Use of Laboratory Animals (2011) by the United States National Academy of Sciences. After acclimatization, the rats were kept in propylene cages at room temperature. The rats were supplied with ordinary food and had unlimited access to water. The animals were arbitrarily split into two groups ($n = 6$).

The administered dose of CLX was 5 mg/kg (Bazan et al., 2016). The first group was administered free CLX dispersed in sodium carboxymethyl cellulose (0.5%), while the second group was administered the optimized CLX-ES-PEI-UENVs. All formulations were delivered orally with adequate water. The animals had free access to food and drank

until the evening before administration, after which they fasted for 12 h. Each rat was fed the oral suspension through stomach intubation, and blood samples were collected at predetermined intervals via retroorbital puncture (1, 2, 3, 4, 6, 8, and 24 h post-dose). Blood was immediately centrifuged (3000 rpm, 10 min) to separate plasma. After collection, the plasma was immediately transferred to plastic tubes (5 mL) and preserved at 20 °C till analysis.

2.7.2. Chromatographic conditions

The quantitative analysis of CLX was determined using a slightly modified LC-MS/MS method (Hu et al., 2021). The LC system consisted of Shimadzu Prominence (Kyoto, Japan) series with degasser (DGU-20A3), an auto-sampler (SIL-20 AC) and a Zorbax C18 column (4.6 × 50 mm; 3.5 μm PS). The mobile phase comprised acetonitrile (80%) and 0.1% formic acid (20%). Ten μL was injected in LC-MS/MS with a flow rate of 1 mL/min. A negative mode was used for CLX and torsemide (internal standard). The autosampler and column temperatures were maintained at 25 °C. Monitoring the transition of the m/z 380.125 precursor ion to the m/z 316.100 for CLX and the m/z 347.196 precursor ion to the m/z 262 for the torsemide was done in the multiple reactions monitoring mode during ion detection. The ion spray voltage was established at 5500 V. The mass spectrometer used was AB Sciex Model (API 3200). Over the concentration range of 2–500 ng/mL, the calibration curve was linear ($R^2 = 0.999$).

2.7.3. Samples preparation

An aliquot of the internal standard (100 μL) in acetonitrile solution (100 ng/mL) was added to the plasma (0.5 mL) containing ethyl acetate (4 mL). The mixture was vortexed, and the solvent was evaporated by a vacuum concentrator and then reconstituted with the mobile phase (0.5 mL). The samples were then centrifuged (3000 rpm) for 10 min, and the supernatant was injected into the LC-MS/MS system.

2.7.4. Pharmacokinetic analysis

The pharmacokinetics of CLX after oral administration of CLX-ES-PEI-UENVs and conventional CLX suspension in rats were analyzed using a non-compartmental model (Aboud et al., 2020). The pharmacokinetic parameters, including area under the curves (AUC), maximum concentration (C_{max}), half-life ($t_{1/2}$), mean residence time (MRT), and peak time (T_{max}) were computed by the PK solver, an add-in program in Microsoft Excel.

2.8. In vivo study of DMH-induced CRC in rats

2.8.1. Animals

The in vivo experimental model was implemented on adult male Wistar rats procured from the animal house of Nahda University, Beni-Suef, Egypt, weighing 200–250 g at the beginning of the protocol. Rats were placed in an air-conditioned (25 ± 1 °C) pathogen-controlled animal room for seven days for adaptation before being subjected to laboratory experiments with free access to standard forage and tap water ad libitum. The experimental protocol for the animal study was approved by the Local Institutional Animal Ethics Committee at Beni-Suef University (Approval no: 022–292).

2.8.2. Experimental design

Rats were arbitrarily assigned into four weight-matched groups, each of 10 rats. The first group was a normal control and given only vehicles. The second group (DMH-induced CRC) was kept as a positive control group and received only DMH (20 mg/kg/S.C) once for 12 weeks (Nascimento-Gonçalves et al., 2021). Group 3 received the DMH + CLX suspension. Group 4 received DMH + the optimal CLX-ES-PEI-UENVs; CLX formulations were given in an oral daily dose after CRC induction within its therapeutic anti-inflammatory dose for rats (5 mg/kg body weight) once for 12 weeks (Bazan et al., 2016). Doses of test agents were decided according to pilot study guided by the published art. At the end

Table 2
Primer sequences for the studied genes.

Gene symbol	Primer sequence from 5′- 3′
β-actin	F: 5-TCCGTCGCCGGTCCACACCC-3
	R: 5-TCACCAACTGGGACGATATG-3
TCF3	F:5-CCAGACCAAACTGCTCATCCTG-3
	R: 5-TCGCCGTTTCAAACAGGCTGCT-3
LEF1	F: 5-CTACCCATCCTCACTGTCAGTC-3
	R: 5-GGATGTTCCTGTTTGACCTGAGG-3

of this experiment, the animals were kept on overnight fasting and sacrificed the following day using sterile instruments under anesthesia with 2.5% thiopental sodium (40 mg/kg, i.p.) before cervical dislocation (Boztaş et al., 2021).

2.8.3. Tissue sampling

Before cervical dislocation, rats were fasted for 24 h. The colon was entirely dissected and washed with saline. Colon was split into two fragments; the first was preserved at −80 °C till the assays of COX-2, Wnt-2, β-catenin, and qRT-PCR analyses for TCF3 and LEF1; the second portion was fixed in 10% formalin in normal saline for a minimum of 48 h until immunohistochemical assay of CXCR 4 and the histopathological assay.

2.8.4. ELISA of tissue biomarkers

Levels of COX-2, Wnt-2 and β-catenin in colon tissue were determined using ELISA test according to the sandwich technique described earlier by Lequin (2005). Absorbance was measured by ELISA Processing System (Model Spectra Max Plus-384 Absorbance Microplate Reader, USA).

2.8.5. Determination of TCF3 and LEF1 expression levels using qRT-PCR

Extraction of total RNA from the colon samples was executed using a Qiagen tissue extraction kit (Qiagen, USA) according to the manufacturer's instructions. Total RNA yield was assessed using NanoDrop® ND-8000 UV–Vis spectrophotometer (NanoDrop Technologies, Wilmington, DE, USA). According to the kit instruction, the extracted RNA was transcribed to cDNA using a high-capacity cDNA reverse transcription kit (ferments, USA). qRT-PCR was implemented using the SYBR Green method. The content of 20 μL reaction mixture was 2 μL cDNA, 10 μL SYBR Green, 1 μL of specific primers (listed in Table 2), and 7 μL nuclease-free water. The PCR conditions were carried out as follows: denaturation at 95 °C for 2 min; followed by 45 cycles at 95 °C for 10 s, 59 °C for 20 s, and 72 °C for 30 s. β-actin was used for the normalization of the target genes data. Data analysis was performed by the 2-ΔΔCT method to compute the relative expression level of the target gene (Livak and Schmittgen, 2001).

2.8.6. Histopathological study

The prepared colon tissue slides were stained with standard Hematoxylin and Eosin (H&E) staining for the histopathological assay according to the method described by Banchroft and Gamble (Bancroft and Gamble, 2008).

2.8.7. Immunohistochemical assay

The immunohistochemical assay of tissue CXCR 4 was executed according to technique designated earlier by Merz et al. (1995) through incubation with primary antibodies against CXCR 4 followed by incubation with secondary antibodies and then with diaminobenzidine/H_2O_2 as a chromogen. Slides were counterstained with hematoxylin then examined under a light microscope with the assistance of a histopathologist.

2.9. Statistical analysis

The data were presented as mean ± SD. SPSS 22 (IBM SPSS Statistics, USA) was used to analyze the data using one-way ANOVA with a Tukey's post-hoc test for multiple comparisons. A p value <0.05 was regarded as significant. The western blot bands were quantified using the Image J computer software (NIH, USA).

3. Results and discussion

3.1. Experimental design and optimization

The results of VS, ZP, PDI, EE, and CR of experimental runs with various Span 80, Tween 80 concentrations, and sonication times are shown in Table 1. The PDI values of CLX-UENVs ranged between 0.069 ± 0.033 and 0.457 ± 0.026 (Table 1). Low PDI values reflect a narrow size distribution and a homogeneous VS pattern, while high PDI values suggest more heterogeneity (Danaei et al., 2018). Analysis of PDI values using ANOVA Type III found insignificant effects on most independent variables. Consequently, PDI was not included in the optimization step.

The wide variety of dependent variable findings suggests that variations in the levels of Span 80, Tween 80, and sonication time may significantly affect UENVs characteristics. Table 3 depicts the mathematical equations with coded values that best represent the causal and response factor interactions. The negligible lack of fit indicates that the models adequately described the observed variance (Table 3). Design-Expert calculated adequate precision to establish the dependability of models used to traverse the design space (Eissa et al., 2022). Adequate precision in the statistical analysis of response variables was more than 4, and predicted R^2 values were close to adjusted R^2 findings. In addition, the ANOVA analysis showed that changes in the levels of Span 80, Tween 80, and sonication time significantly affected the response variables. Fig. S1 (supplemental file) shows the diagnostic model plots that prove the appropriateness of the fitted models.

3.1.1. Analysis of vesicle size (VS)

Actually, tumor cells create a neovasculature to guarantee a sufficient resource of nutrients and oxygen. As tumors enlarge, they recruit new vessels or engulf current blood vessels. Tumor vasculature is different from normal blood vessels as it is deficient of complete endothelial lining with relatively large pores (0.1–3 μm in diameter) resulting in markedly greater vascular permeability. Nanoparticles are capable of penetration via the infirmly compacted vasculature to be delivered to the tumor microenvironment and remain there due to the inadequate lymphatic drainage of tumors. This phenomenon called enhanced permeability and retention effect (EPR) which highlighted the possibility to utilize nano-sized drugs to passively target tumors (Nakamura et al., 2016). Moreover, VS determines the cellular absorption, biodistribution and circulation half-life of the nanosystem. Small-sized nanovesicles can be absorbed to a better extent than bigger ones due to the fact that cellular uptake of the nano-cargo is size dependent (Salem et al., 2022).

VS analysis was carried out to reinforce the nanoscale range of the resultant nanovesicular dispersions. According to Table 1, the VS of the developed nanovesicular formulations ranged from 129.53 ± 10.85 to 267.81 ± 2.96 nm. EAs-contained vesicles are typically spherical, have a low propensity to agglomerate, and hence have small sizes (Aboud et al.,

Table 3
The outcomes of ANOVA analyses of response variables by the design expert software.

Source	VS		ZP		EE		CR	
	F-value	*p*-value	F-value	p-value	F	p-value	F	p-value
Model	77.28	< 0.0001	38.98	< 0.0001	404.12	< 0.0001	1106.19	< 0.0001
X_1: Span 80	190.21	< 0.0001	95.13	< 0.0001	2798.32	< 0.0001	8266.67	< 0.0001
X_2: Tween 80	33.83	0.0001	21.79	0.0007	60.05	< 0.0001	1187.56	< 0.0001
X_3: Sonication time	7.81	0.0174	0.0329	0.8593	56.12	< 0.0001	65.47	< 0.0001
$X_1. X_2$					20.07	< 0.0001	91.66	< 0.0001
$X_1. X_3$					16.08	0.0003	16.61	0.0003
$X_2. X_3$					13.43	0.0009	3.74	0.0618
X_1^2					488.37	< 0.0001	229.46	< 0.0001
X_2^2					165.40	< 0.0001	69.87	< 0.0001
X_3^2					26.26	< 0.0001	1.73	0.1976
Lack of Fit	0.8665	0.6420	1.22	0.5287	13.46	0.0709	0.8236	0.6392
Model	Linear		Linear		Quadratic		Quadratic	
Adjusted R^2	0.9424		0.8906		0.9886		0.9958	
R^2	0.9547		0.9140		0.9910		0.9967	
%CV	4.36		7.84		1.80		1.81	
Predicted R^2	0.9158		0.8419		0.9821		0.9943	
Adequate precision	26.8490		19.7472		59.25		102.57	
Standard deviation	8.95		0.8377		1.42		1.12	

$$VS = 205.5 - 43.7.X_1 - 18.4.X_2 - 8.9.X_3$$

$$ZP = 10.7 + 2.9.X_1 - 1.4.X_2 - 0.054.X_3$$

$$EE = +85.54 + 15.29X_1 + 2.24X_2 - 2.17X_3 - 1.86X_1X_2 + 1.64X_1X_3 + 1.50X_2X_3 - 9.40X_1^2 - 5.47X_2^2 + 2.18X_3^2$$

$$CR = +60.73 + 20.72X_1 + 7.85X_2 + 1.84X_3 + 3.08X_1X_2 + 1.31X_1X_3 + 0.6229X_2X_3 + 5.08X_1^2 - 2.80X_2^2 - 0.4410X_3^2$$

2020). Following transformation, the linear model was suggested for VS data. The influence of Span 80, Tween 80, and sonication time on the VS of CLX-UENVs formulations is shown in Fig. 1(A, B, and C). The VS decreased as the level of Span 80, Tween 80, and sonication time increased.

As illustrated in Fig. 1(A, B), VS was decreased while increasing the levels of Span 80. Indeed, the lower the HLB of the surfactant, the smaller the VS generated. The observed link between the size of nano-vesicles and HLB may be explained by reduction of surface energy brought by increased hydrophobicity, resulting in smaller vesicles (Khallaf et al., 2020). These findings were similar to those narrated by Khallaf et al. (2020). Notably, EA (Tween 80) levels had a substantial antagonistic effect on the mean VS. This may be interpreted as a decrease in interfacial tension with increasing surfactant concentrations, resulting in the formation of small VS. In contrast, a low level of EA may be unable to cover the whole diameter of the vesicles. Therefore, vesicle agglomeration may occur when the surface area is reduced to the point that the EA may continue to exist throughout the whole surface of the aggregation, creating bigger particles (Al-Mahallawi et al., 2017). Mahmoud et al. (2017) found comparable findings during the preparation of atorvastatin-loaded nanovesicular systems. As expected, increasing the time of sonication decreased the VS, as shown in Fig. 1(B, C). This may occur as a consequence of the exposure of the vesicles to ultrasonic vibrations, leading to vesicle fragmentation (Elsherif et al., 2017). Such observations are supported by previous research findings (El-Say et al., 2016; El Menshawe et al., 2019).

3.1.2. Analysis of zeta potential (ZP)

ZP is the overall charge that vesicles have attained which can be considered as an indirect measurement for the judgment of colloidal dispersions stability (Albash et al., 2019). High surface charge values may prevent nanoparticles from aggregation by imbuing their surfaces with greater repulsion forces (Eid et al., 2021). The ZP values in Table 1 ranged between −5.02 ± 0.20 and − 13.83 ± 0.47 mV. Since all the formulations in this study had negative ZP values, variation in ZP will be argued in terms of its absolute value to avoid misperception. It was determined that the linear model was adequate for assessing the ZP data. ANOVA Type III-Partial Analysis demonstrated significant effects of Span 80 and Tween 80 on ZP values ($p < 0.05$), although sonication time had no significant influence on ZP values.

Of note, the ZP of vesicles reduced upon using Tweens instead of Spans which might be assigned to the elevated HLB value of Tween 80 (15) compared to Span 80 (4.3). As shown in Fig. 1(D, E), when the level of Span 80 was increased from 160 to 200 mg, ZP rose from |5.02| to | 13.83| mV. This may result from the rising OH ion level, which is utilized to achieve high ZP (Abdelbari et al., 2021). In addition, the ZP values declined gradually as the EA level increased which might be resulted from the accumulation of hydrophilic EA on vesicular bilayers, resulting in the shielding of negative surface charges (Basha et al., 2013). Kim et al. (2000) claimed that the HLB value of the surfactant impacts the competitive adsorption of OH ions at the interface that are existent in the hydration milieu. The lower HLB value of the surfactant (the nonpolar interface is more), the increased adsorbed OH which in turn raises ZP. Moreover, the existence of $(CH_2\text{-}CH_2\text{-}O)_n$ in Tweens created hydrogen bonds with water particles led to lower ZP values (Ibrahim et al., 2015). Our outcomes are concurred with those stated by Albash et al. (2019).

3.1.3. Analysis of entrapment efficiency (EE)

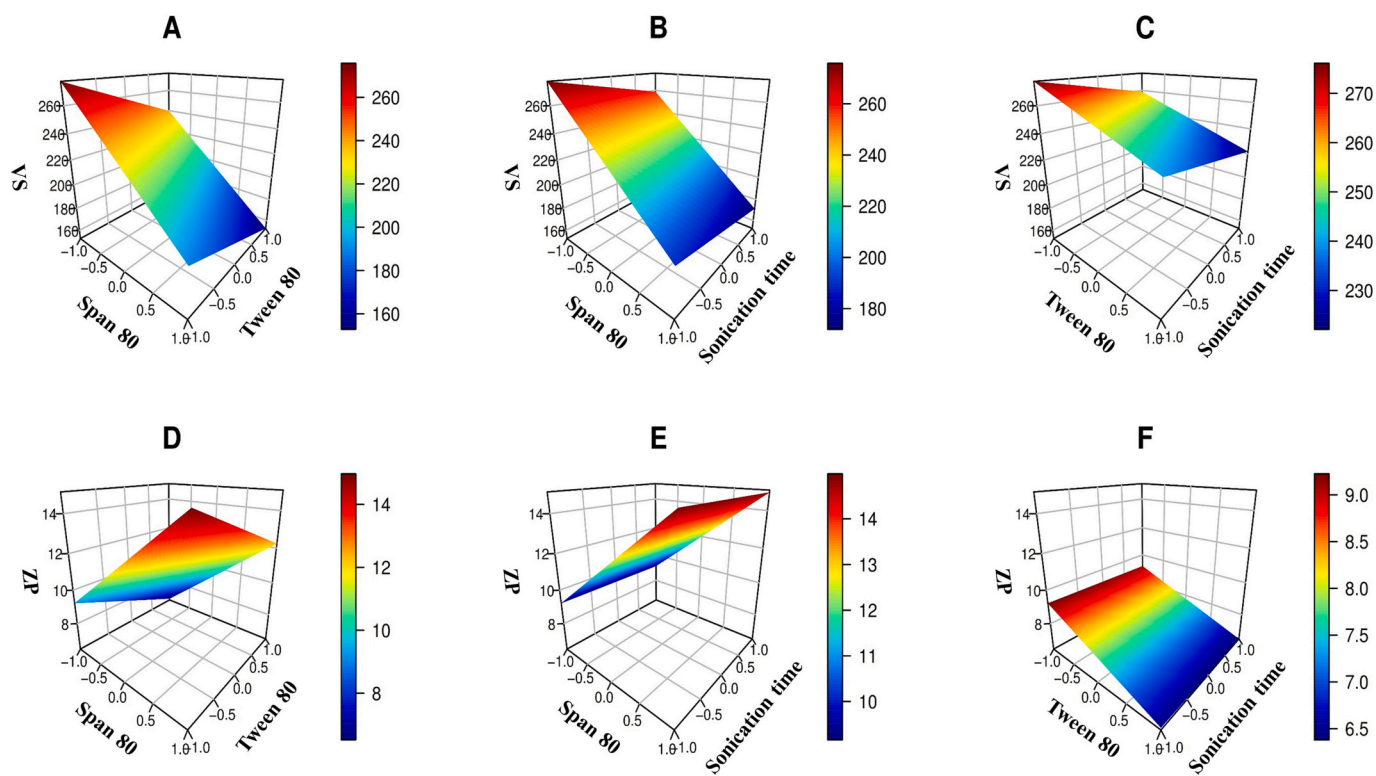As elicited in Table 1, the developed CLX-UENVs formulations had

Fig. 1. 3D plots for the impacts of independent variables on size (VS) and zeta potential (ZP) of CLX-UENVs.
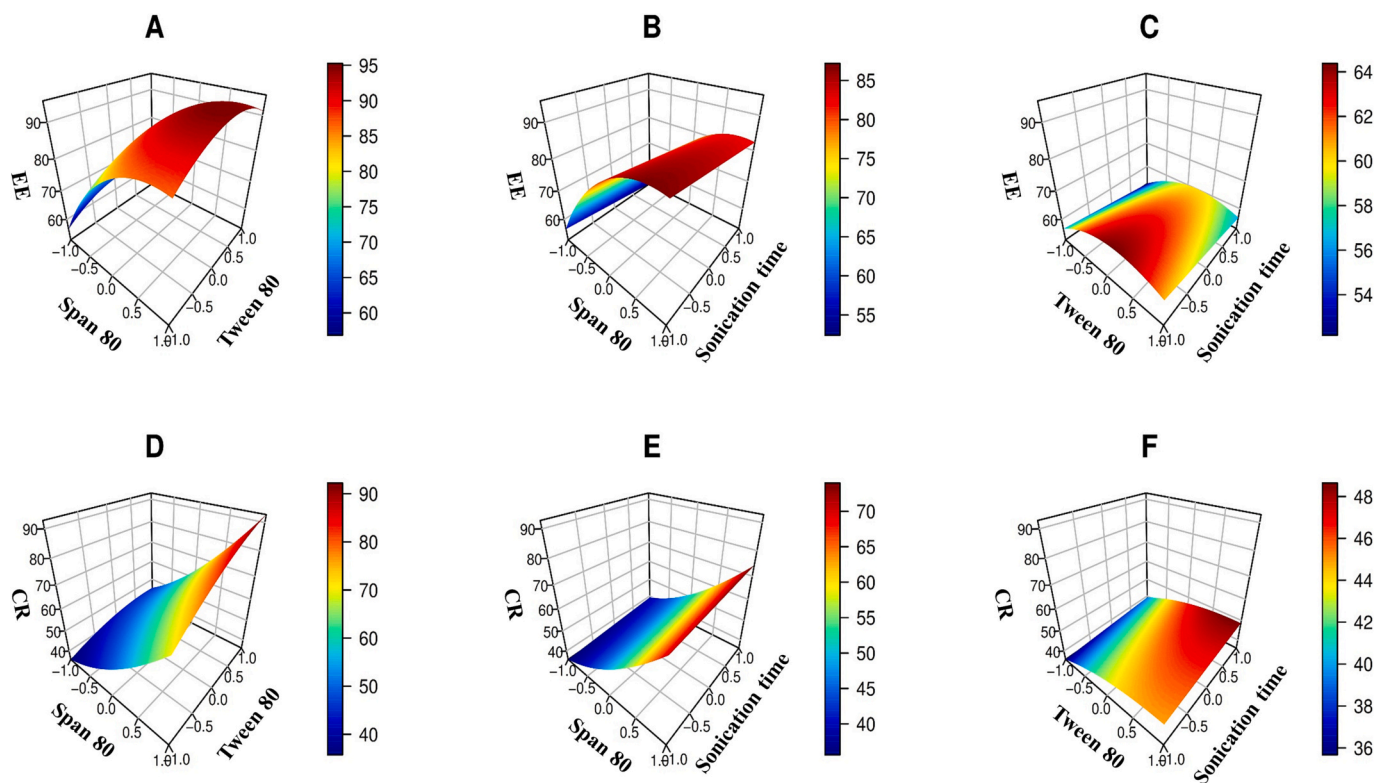

Fig. 2. 3D plots for the impacts of independent variables on entrapment efficiency (EE) and cumulative release after 24 h (CR) of CLX-UENVs.

EE that ranged from 50.03 ± 3.21 to 93.07 ± 2.57%. The quadratic model was recommended for the analysis of entrapment data. The three independent factors substantially impacted the entrapment of CLX inside CLX-UENVs ($p < 0.05$). According to the regression results, Span 80

and Tween 80 disclosed a significant positive impact on the EE% results. In contrast, the encapsulation of CLX was negatively affected by the sonication time.

As shown in Fig. 2(A-C), more than 90% of entrapment was obtained

when Span 80 level was more than 190 mg and Tween 80 at more than 15%. The entrapment values increased when the levels of Span 80 were raised which might be deduced based on the length of the alkyl chain, which affords high drug encapsulation (El Menshawe et al., 2019). In addition, increasing the quantity of Span 80 (a vesicle-forming material) may lead to the creation of a more lipophilic environment to house a higher quantity of the hydrophobic drug (CLX), hence boosting the EE% (Aziz et al., 2018). Concerning the influence of Tween 80, ANOVA analysis indicated that nanovesicles created with high Tween 80 levels had a higher EE% than those prepared with low levels. The ability of EA, when used optimally, to give more space for retaining more medications may explain the positive effect of EA on encapsulation (El Menshawe et al., 2019). It may also be linked to the ability of the EA to create a stabilizing coating over the formed vesicles. Additionally, this coat may hold more drugs, raising the entrapment (Aboud et al., 2018). In contrast, the fluidizing effect of EA at high amounts on the vesicle bilayers may have led to the liberation of the entrapped drug (Eid et al., 2019; Elkomy et al., 2022a; Elkomy et al., 2022b).

As shown in Table 3 and Fig. 2(B, C), it was also evident that the sonication duration had an inverse marked impact on the entrapment, $p < 0.05$. This may be a consequence of the rupture and reaggregation of vesicles, which results in micellar solubilization rather than entrapment of the medication inside nanovesicles (El Menshawe et al., 2019). This result is congruent with the results of Andersen et al. (2013) who showed a decline in entrapment as sonication duration increased during the formation of chitosomes and pectosomes for metronidazole delivery.

3.1.4. Analysis of cumulative release (CR)

The cumulative release (CR) data after 24 h of all the assembled CLX-UENVs formulations are presented in Table 1. The CR after 24 h ranged between 38.26 ± 5.06 and $93.92 \pm 4.19\%$. The current study demonstrated that UENVs are ideal reservoirs for CLX. The quadratic model was recommended for the CR data analysis. From the regression coefficients, the levels of Span 80, Tween 80, and the time of sonication significantly impacted CR values, $p < 0.05$.

Concerning Span 80, it was observed that a high CR was produced when Span 80 levels were elevated (Fig. 2D and E). Rapid release at high levels of Span 80 might be due to the existence of an unsaturated alkyl chain, facilitating CLX leakage (El Menshawe et al., 2019). Furthermore, Span 80 had a low phase transition temperature ($-12\ °C$), resulting in an increasing CR (El Menshawe et al., 2019). Notably, high Tween 80 levels led to a high release rate. This is because Tween 80 has a short alkyl chain length, resulting in a fast release rate (Devaraj et al., 2002). Moreover, the reduced VS of UENVs with high levels of Tween 80 may expose a larger surface area to the release environment, hence boosting drug release. Additionally, CR data analysis showed that sonication had a markedly positive impact on the CR of CLX-UENV formulations. The VS may assert this positive link between sonication time and CR. At any given moment, the fraction of the drug dissolved in the aqueous environment has an inverse correlation with the vesicle diameter. Thus, the smaller VS might reduce the diffusional distance, thus accelerating drug release rates (Wacker, 2013).

Kinetic analysis of CLX release data via linear regression elicited that the drug was released from the majority of the UENVs dispersions by Higuchi kinetics elucidating a diffusion-controllable pattern, Table S1 (supplemental file). Diverse reports disclosed that drug-loaded vesicular

nanosystems would follow a controlled-release mechanism congruent with Higuchi plots (Aboud et al., 2018; El Menshawe et al., 2019; Salem et al., 2022).

3.2. Formulation optimization

The Design Expert® software made a number of recommendations that optimally fulfilled the specified constraints (minimum VS, and maximum ZP, EE, and CR). The optimized formulation (X_1: Span 80: 200 mg, X_2: Tween 80: 25.7% (w/w), and X_3: Sonication time: 10 min) had a desirability value of 0.92. The experimental, expected, and prediction errors for the response variables of the optimal CLX-UENVs formulation are manifested in Table 4. In addition, the computed percentage of prediction error for entire dependent variables was fewer than 11%. These results proved the validity of the ultimate models.

The standardized relative influences of the formulation parameters on the response variables are demonstrated in the Pareto chart (Fig. S2, supplemental file). VS, ZP, EE, and CR were more affected by Span 80 levels than by Tween 80 or sonication time.

3.3. Characterization of CLX-ES-PEI-UENVs

3.3.1. VS, PDI, ZP, and EE analysis

The addition of PEI caused the VS to increase from 147.53 ± 11.44 to 176.81 ± 16.63 nm, and ZP shifted from -15.40 ± 0.21 to $+2.69 \pm 0.09$ mV. The inclusion of ES as a pH-sensitive layer altered the ZP from positive ($+2.69$) to negative (-23.24 ± 0.48 mV) and increased the VS from 176.81 to 253.62 ± 18.45 nm, suggesting the successful production of CLX-ES-PEI-UENVs. ZP decreased after PEI surface coating, possibly due to the creation of a dense polymer layer that neutralized the accumulated negative charge on CLX-UENVs. After surface coating with ES, the ZP exhibited negative ZP again due to the anionic nature of ES. CLX-ES-PEI-UENVs depicted a PDI of 0.282, showing a narrow size distribution. The EE of CLX within CLX-ES-PEI-UENVs ($85.64 \pm 3.64\%$) was slightly lower than that of CLX-UENVs ($87.27 \pm 3.06\%$) and CLX-PEI-UENVs ($86.96 \pm 4.57\%$). This might be attributed to a leak of the encapsulated CLX during the ES layer addition procedure.

3.3.2. Morphological evaluation

As elucidated in Fig. 3, the TEM revealed the morphology of CLX-UENVs, CLX-PEI-UENVs, and CLX-ES-PEI-UENVs. All UENVs formulations displayed spherical structures devoid of cracking and aggregation. Upon comparison of TEM micrographs and Zetasizer data, the average VS via TEM micrographs was comparable to that recorded with DLS.

3.3.3. pH-dependent drug release and ZP

In the stomach condition, CLX-UENVs and CLX-PEI-UENVs demonstrated an early burst drug release (more than 40% after 2 h), followed by an extended-release in the upper site of the small intestine condition, as presented in Fig. 4. In the first 6 h, more than 65% of CLX was released from CLX-UENVs and CLX-PEI-UENVs. CLX-ES-PEI-UENVs, on the other hand, only released 18% of CLX in the first 6 h (6.4% in the stomach), showing that they could limit the CLX release in the upper GIT. The release of CLX from CLX-ES-PEI-UENVs was much more rapid at the terminal ileum (pH 7.4) than at acidic pH values. CLX-ES-PEI-UENVs surface charge reversal property was evaluated in a milieu simulating the stomach, small intestine, colon and rectum pH conditions. In an acidic environment, CLX-ES-PEI-UENVs retained a negative surface charge, which they changed to a positive superficial charge in a milieu with a higher pH by dissolving the negatively charged ES layer.

It's interesting to note that CLX-ES-PEI-UENVs were designed for intelligent charge reversal (from negative to positive), which prevents undesirable mucus adhesion before reaching the colorectal segments, restricts early burst release of CLX in the upper GIT, and then improves the accumulation of nanovesicles and prolongs the release of CLX in the target regions. The distinctive pH-triggered characteristic of surface

Table 4
The results of dependent variables (software predicted, experimental, and prediction error) of the optimized CLX-UENVs.

	VS (nm)	ZP (mV)	EE%	CR % (24 h)
Predicted	142.42	-13.71	89.68	93.45
Experimental	147.53	-15.40	87.27	93.94
Prediction error (%)[£]	3.46	10.97	-2.76	0.52

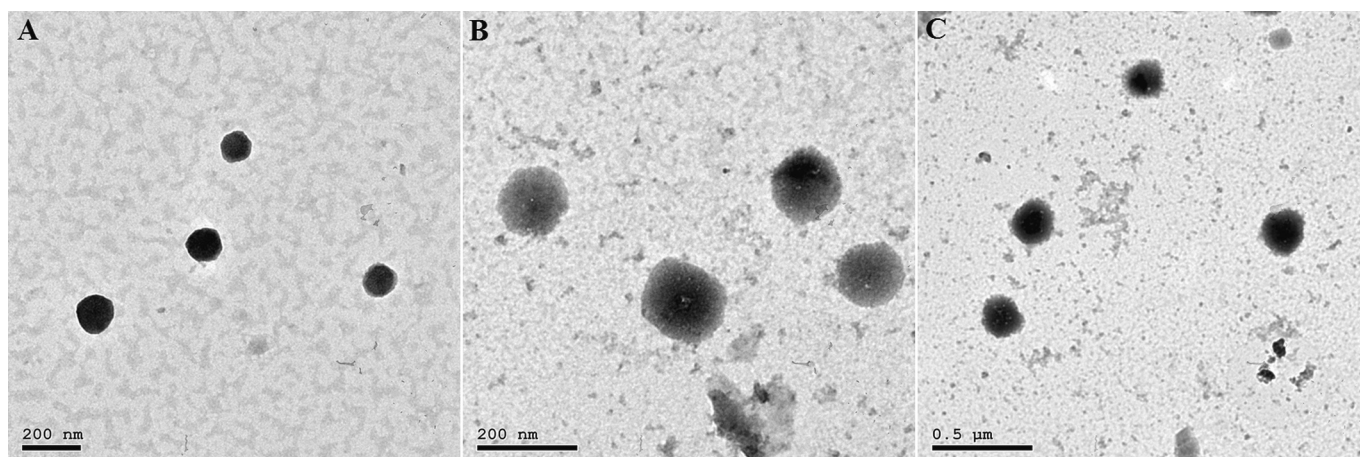[£] (Experimental – Predicted) / Experimental x 100.

Fig. 3. TEM morphology of CLX-UENVs (A), CLX-PEI-UENVs (B), and CLX-ES-PEI-UENVs (C).
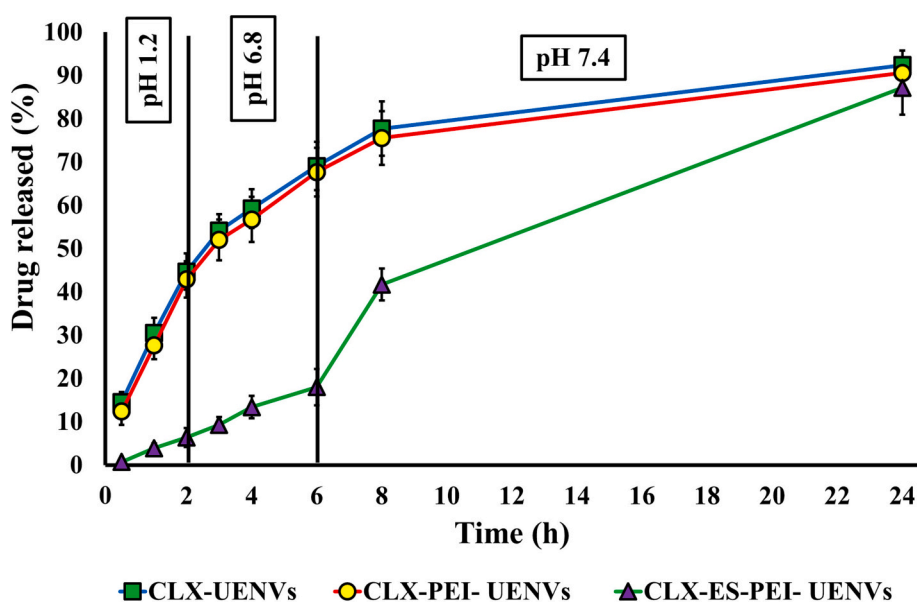

Fig. 4. In vitro release profiles of CLX from CLX-UENVs, CLX-PEI-UENVs, and CLX-ES-PEI-UENVs.

charge reversal would lead to greater CLX levels in the colorectal region, enhancing therapeutic efficacy (Niebel et al., 2012).

3.3.4. Short-term stability

After storing for three months at 4 °C, the optimized CLX-ES-PEI-UENVs formulation had a milky appearance with no separation, aggregation, or precipitation. In addition, the changes in size, entrapment, or surface charge are insignificant during the storage period, as illustrated in Fig. 5. The high stability of CLX-ES-PEI-UENVs may be attributed to their nanoscale range and high ZP (-23.24).

3.4. In vivo pharmacokinetic studies

Fig. 6 manifests the CLX plasma concentration-time curves after CLX suspension and CLX-ES-PEI-UENVs administration to rats. Table 5 displays the various pharmacokinetic characteristics of the two administered formulations after oral delivery. Following oral administration of CLX suspension, C_{max} (480.51 $\pm$ 115.94) was reached in 3.17 $\pm$ 0.41 h; however, the plasma levels of CLX dropped off quickly. Whereas following administration of CLX-ES-PEI-UENVs, a comparatively slow rise and sustained plasma levels of CLX for a longer duration were detected, with delayed C_{max} (764.19 $\pm$ 23.91) occurring at 4.67 $\pm$ 0.94 h, indicating an evidently regulated release of CLX from the CLX-ES-PEI-UENVs. Additionally, the delay in mean T_{max} from 3.17 h (CLX suspension) to 4.67 h (CLX-ES-PEI-UENVs) might be related to the capacity of ES to shield the entrapped CLX from the anticipated breakdown in the stomach. After the fast stomach emptying of this aqueous dispersion, the enteric coat will disintegrate quickly at the pH of the duodenum within 15 to 30 min (Kendall et al., 2009; Tayel et al., 2015). These may be assisted by the enormous surface area of the duodenum, the amorphous form of the entrapped medication, and the great dispersion level of the drug (Tayel et al., 2015).
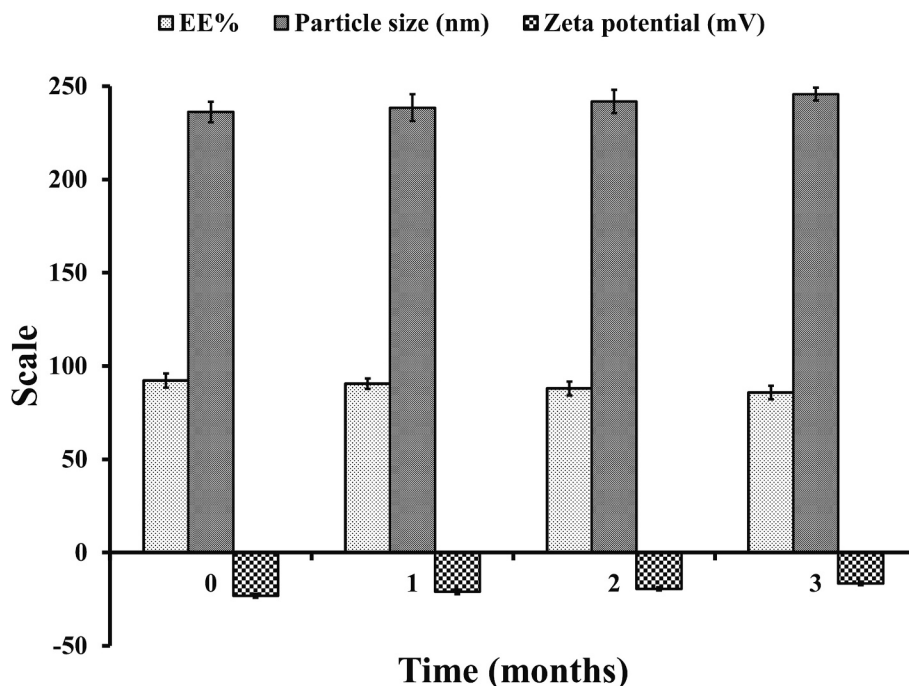
□EE% ■Particle size (nm) ⊠Zeta potential (mV)

Fig. 5. The mean VS, EE, and ZP of the optimized CLX-ES-PEI-UENVs formulation after 0, 1, 2, and 3 months of storage in the refrigerator (4 °C).
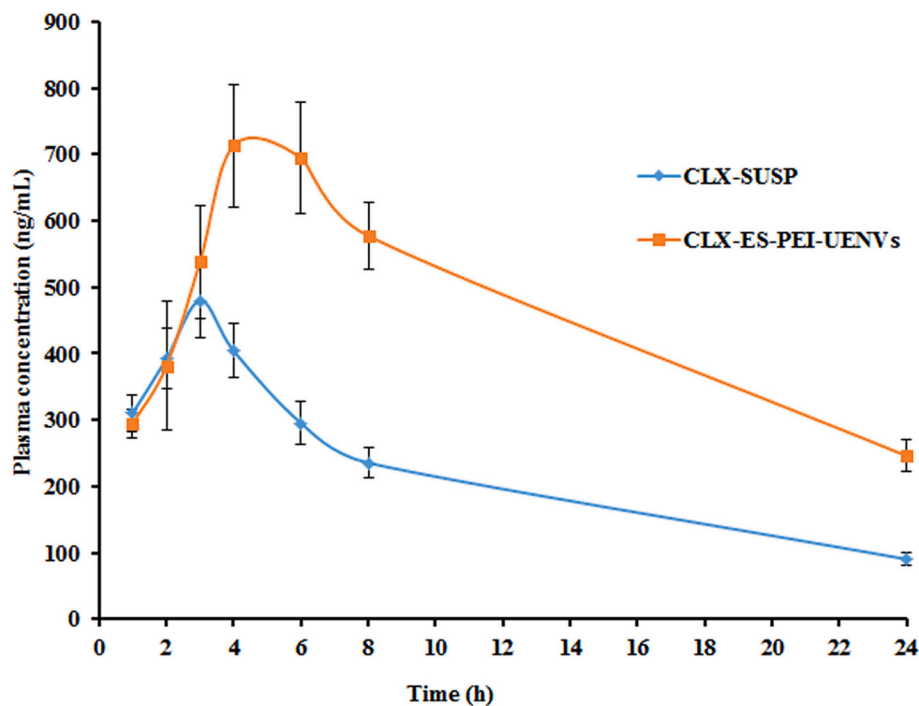

Fig. 6. CLX levels in rat plasma following oral administration of CLX suspension and CLX-ES-PEI-UENVs.

The prolongation in the MRT from 15.45 ± 1.99 to 18.98 ± 1.03 h as well as in the elimination half-life from 11.06 ± 0.93 to 12.44 ± 0.55 h for CLX suspension and CLX-ES-PEI-UENVs, respectively, could imply the sustained release features of the fabricated nano-cargo. Depending on the computed AUC_{0-24} values of CLX suspension (5068.40 ± 1577.32 ng.h/mL) and CLX-ES-PEI-UENVs ($10{,}840.11 \pm 790.29$ ng.h/mL), the CLX oral bioavailability was observed to be increased by approximately 2.13-fold. The improved oral bioavailability may be due to the potential of CLX-ES-PEI-UENVs to carry drugs to the duodenal site of absorption, offer transient drug protection from the acidic medium, and minimize

hepatic metabolism besides the permeation enhancing traits of the crafted nano-cargo. The enhanced bioavailability may help the CRC patient by lowering the therapeutic dose or increasing drug efficacy (Tayel et al., 2015).

3.5. In vivo study of DMH-induced CRC in experimental rats

3.5.1. Effect of different CLX formulations on inflammatory markers (COX-2 and IL-1β) levels

The average value results of rats exposed to DMH disclosed

Table 5

Pharmacokinetic parameters of CLX after oral delivery of CLX suspension and CLX-ES-PEI-UENVs with the CLX dose of 5 mg/kg.

Parameter	CLX suspension	CLX-ES-PEI-UENVs
$T_{1/2}$ (h)	11.06 ± 0.93	12.44 ± 0.55[a]
K (h^{-1})	0.0627 ± 0.0045	0.0557 ± 0.0024[a]
T_{max} (h)	3.17 ± 0.41	4.67 ± 0.94[a]
C_{max} (ng/mL)	480.51 ± 115.94	764.19 ± 23.91[a]
Mean Residence Time (h)	15.45 ± 1.99	18.98 ± 1.03[a]
AUC_{0-24} (ng h/mL)	5068.40 ± 1577.32	$10,840.11 \pm 790.29$[a]
$AUC_{0-\infty}$ (ng h/mL)	6530.75 ± 2806.22	$15,257.09 \pm 1148.91$[a]
F_{rel} (%)	–	213.88

$T_{1/2}$: terminal half-life; K: elimination rate constant; T_{max}: time to reach C_{max}; C_{max}: maximum drug concentration in plasma; MRT: mean residence time; AUC_{0-24}: area under plasma concentration–time curve from 0 to 24 h; $AUC_{0-\infty}$: total area under plasma concentration–time curve; F_{rel}: relative bioavailability. Listed data are mean values ($n = 6$) $\pm$ SD.

Using one-way ANOVA followed by Tukey's post-hoc test.

[a] $p < 0.05$ versus oral CLX suspension.

Table 6

Colonic COX-2, IL-1β, Wnt-2 and β-catenin levels in different studied groups.

Group	COX-2 (pg/g tissue)	IL-1β (pg/g tissue)	Wnt-2 (pg/g tissue)	β-catenin (pg/g tissue)
Control	136.76 ± 2.53	43.37 ± 2.59	5.94 ± 0.23	7.78 ± 0.24
DMH	489.24 ± 20.09[a]	263.83 ± 26.67[a]	1.27 ± 0.15[a]	2.81 ± 0.32[a]
CLX suspension	283.86 ± 14.49[a,b]	70.90 ± 9.51[b]	2.89 ± 0.14[a,b]	4.19 ± 0.24[a,b]
CLX-ES-PEI-UENVs	181.18 ± 4.04[b,c]	60.77 ± 3.54[b]	3.77 ± 0.3[a,b]	5.58 ± 0.35[a,b]

Data are expressed as mean $\pm$ SD with n = 10 for each group.

Using one-way ANOVA followed by Tukey's post hoc test.

[a] Significantly differs from the control group.

[b] significantly differs from the DMH group.

[c] significantly differs from the CLX suspension group at $p < 0.05$.

significantly elevated inflammation signs in colon tissue homogenate levels of COX2 and IL-1β to 357.73% and 608.38%, respectively, compared to normal control rats. Besides, treated groups received CLX suspension for 12 weeks revealed a reduction in the intensity of inflammatory tissue signs for COX2 and IL-1β by 58.02% and 26.87%, respectively compared to DMH tissue levels. On the other hand, the treatment with CLX-ES-PEI-UENVs for 12 weeks markedly ameliorated both COX2 and IL-1β tissue levels compared to DMH induction group tissue levels, Table 6.

Our results indicated the effect of CLX-ES-PEI-UENVs nanodispersion in the treatment of animals aggressive inflammation and immunological disorder from DMH-induced CRC. Previous data claimed that DMH induced oxidative stress release coupled with apoptotic cells and various inflammatory markers including nuclear factor kappa (NF-κB), interleukines (IL-6 and IL-1β) and COX-2 (Babu et al., 2023). Importantly, arts have shown that CLX can block the expression and activation of NF-κB and that it can fight off wide variety of molecules that contribute to the expression, production, and secretion of inflammatory responses. These molecules include tumor necrosis factor alpha (TNF-α), IL-1β, IL-6, IL-8, COX-2 (Ferreira et al., 2021). A recent report has shown that the selective overexpression of COX-2 in colon cancers has been related to the development of malignant tumors (Samadarsi et al., 2022). Such observation suggests that inhibiting COX-2 will significantly decrease

the occurrence of CRC as mentioned in the American Cancer Society reports on the rate of CRC in patients with inflammatory bowel ailment (Lee et al., 2021). Similarly, ovarian cancer model involved a great expression of COX-2, promoting the cancer metastasis via stimulating the phosphorylation of NF-κB, up-regulating the expression of C-myc and phosphorylated STAT, and snowballing the expression of MMP-2, MMP-9 and IL-1β (Zhang et al., 2019). Moreover, recent mesenchymal stem cells (MSCs) studies suggest alternative CLX management for patients with irritable bowel disease as a CRC precursor (Borowczak et al., 2022). The MSCs migration towards CRC cells represents a wide suppression of immunological, inflammatory and apoptotic markers (Wang et al., 2023).

Migration of MSCs to areas of tissue injury/inflammation has been previously proven (Sadighparvar et al., 2020; Nascimento-Gonçalves et al., 2021). Inflammatory cytokines like interferon gamma (IFN-γ), TNF-α, or IL-1, provoke MSCs at injury sites to express a wide variety of immunosuppressive factors through their ability to release PGE2 (Zhang et al., 2019). Indeed, in mouse models of colon carcinogenesis, the size and quantity of adenomas are significantly reduced once COX-2 is inhibited, either pharmacologically or through genetic disruption (Assoni et al., 2022). Alongside, it has been declared that signaling for TNF-α and IL-1β are two pathways that are typically dysregulated in autoimmune disorders and cancer (Zhao et al., 2021). Besides, researchers have demonstrated that both signaling cascades directly control arachidonic acid pathway and selectively stimulate the expression of PGE2-generating enzymes (Monteleone and Lutz, 2021). All these data confirmed our results that CLX has potent anti-inflammatory and immunomodulatory effects, Table 6.

3.5.2. Effect of different CLX formulations on Wnt-2/β-catenin levels

The Wnt-2/β-catenin pathway is strictly related to the incidence and growth of tumors. Our data reveal that rats subjected to DMH showed an aggressive downregulation in colon tissue mean value levels of Wnt-2/β-catenin $1.27 \pm 0.23/2.81 \pm 0.32$ by 21.42% and 36.12%, respectively compared to normal control rats. In contrast, CLX suspension exhibited re-enhancement in Wnt-2/β-catenin tissue mean value levels to $2.89 \pm 0.15/4.19 \pm 0.24$; while the group received 12 weeks of treatment with CLX-ES-PEI-UENVs enhanced Wnt-2/β-catenin mean tissue levels more than DMH-induced CRC and CLX suspension levels to $3.76 \pm 0.31/5.58 \pm 0.35$ (Table 6).

Recent arts have displayed that Wnt-2/β-catenin is included in the progression of numerous types of human carcinogenicity (Tewari et al., 2021; Hiremath et al., 2022). Researchers found that β-catenin mRNA was much higher in frontline invasive CRC cells indicating its regulatory role in adherence junctions for hemophilic cell to cell adherence. In addition, it is involved in cell signaling and gene transcription (Yuan et al., 2021). Indeed, the absence of Wnt-2 results in a lack of β-catenin and subsequently interferes with autophagy-promoting factors and stimulates transcription of many signaling pathways involved in cell proliferation (Lin et al., 2020) associated with many human diseases such as gastric, colon, and liver cancer (Flanagan et al., 2015). Many inflammatory tumors have demonstrated a cross talk among the inflammatory cascade and the Wnt/β-catenin signaling pathway (Tewari et al., 2021). In addition, microorganisms causing infections can cause unchecked inflammation by overexpressing the Wnt/β-catenin pathway, which can ultimately raise the risk of carcinogenesis (Anuja et al., 2017). In parallel, Wnt/β-catenin downregulation could stimulate the production of several inflammatory markers like COX-2 (Sobolewski et al., 2010), triggering overexpression of oxidative stress and numerous cytokines production that enhance apoptotic factors and metastasis
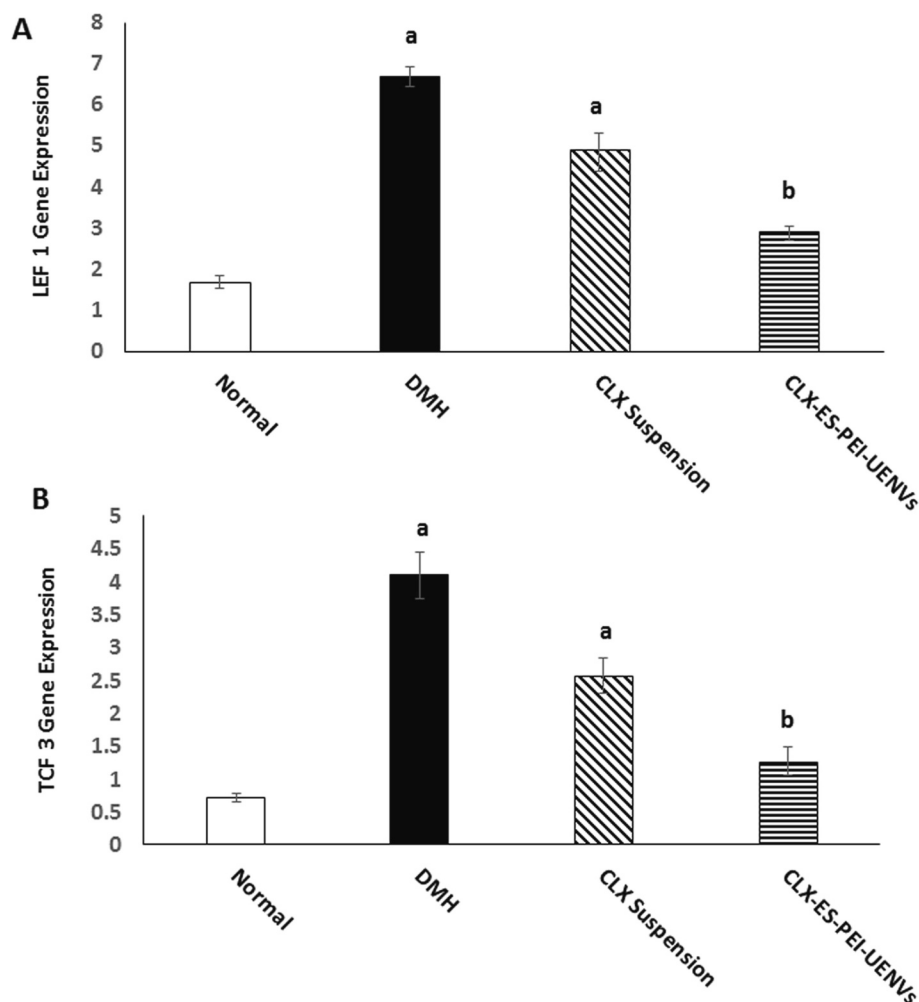
Fig. 7. Colonic LEF 1 (A) and TCF 3 (B) gene expression levels in different studied groups. Data were expressed as mean $\pm$ SD with $n = 10$ for each group using one-way ANOVA followed by Tukey's post hoc test. [a] Significantly differs from the control group, [b] significantly differs from the DMH group, [c] significantly differs from the CLX suspension group at $p < 0.05$.

(Nigam et al., 2023). Finally, our experimental results are congruent with previous researches that targeted the effect of COX-2 inhibitors towards the crosslink of upregulating the Wnt/β-catenin pathway.

### 3.5.3. Effect of different CLX formulations on LEF 1/TCF 3 gene expression

The in vivo experimental LEF 1/TCF 3 gene expression results indicated that the DMH-induced CRC upregulated LEF 1/TCF 3 expression in colon tissues by 394.12% and 576.06%, respectively compared to normal control rats. In addition, the rat group received CLX suspension showed a significant improvement for LEF 1 expression by 72.83% and TCF 3 by 62.84% compared to DMH-induced CRC group. On the other hand, treatment with CLX-ES-PEI-UENVs displayed a significant improvement in LEF 1/TCF 3 gene expression compared to both CLX suspension and DMH-induced CRC groups (Fig. 7A, B).

The T cell factor/lymphoid enhancer family genes encode for DNA transcription factors via the SRY-related high mobility group (SOX) domain (Liu et al., 2017). They have been involved in many diseases such as cancer (Peschel et al., 2022), and beta cells homeostasis (Locke et al., 2011; Peschel et al., 2022). Additionally, they are involved in the Wnt signaling pathway (Takamoto et al., 2014). A model for breast cancer manifested that upregulation of Wnt 3 induced a downregulation of LEF 1/TCF 3 expression that inhibited cancer cells metastasis and progression (Kaiser et al., 2023). Also, the cisplatin-induced ovarian cancer model demonstrated that the down-regulation of LEF 1/TCF 3

suppressed multicellular pathways related to ovarian cell carcinoma (Huang et al., 2023). Alongside, Zhou et al. (2017) exhibited that downregulation of MDR1/P-gp and inhibition of the Wnt/β-catenin signaling pathway with miR-506 augmented CRC cell sensitivity to oxaliplatin and induced upregulation of LEF 1/TCF 3 cascade. Prostate cancer model also manifested that β-catenin signaling promoted phosphorylation of GSK-3 that engaged to the c-Myc promoter and interacted with TCF4 independent of β-catenin resulting in increased cancer cell transcription (Schneider and Logan, 2018). Xia et al. (2010) reported that treatment with CLX inhibited the β-catenin-dependent surviving activity of the osteosarcoma cell line. According to the previous research, our results could be promising in the management of CRC by CLX via regulation of Wnt/β-catenin/LEF 1/TCF 3 expression levels which is involved in disease progression and metastasis.

3.5.4. Effect of different CLX formulations on CXCR4 immunohistochemical staining

Normal control group colon sections showed negative reactivity for CXCR4. The DMH CRC group showed an intense expression of CXCR4 in the colon mucosa. CLX suspension treatment showed moderate positive staining for CXCR4; while CLX-ES-PEI-UENVs showed a very mild to limited expression of CXCR4 in the colon wall (Fig. 8A-D). Katoh et al. (2010) observed that inhibition of COX-2 diminished CXCL12/CXCR4 expression besides expression of multiple other chemokines among lung
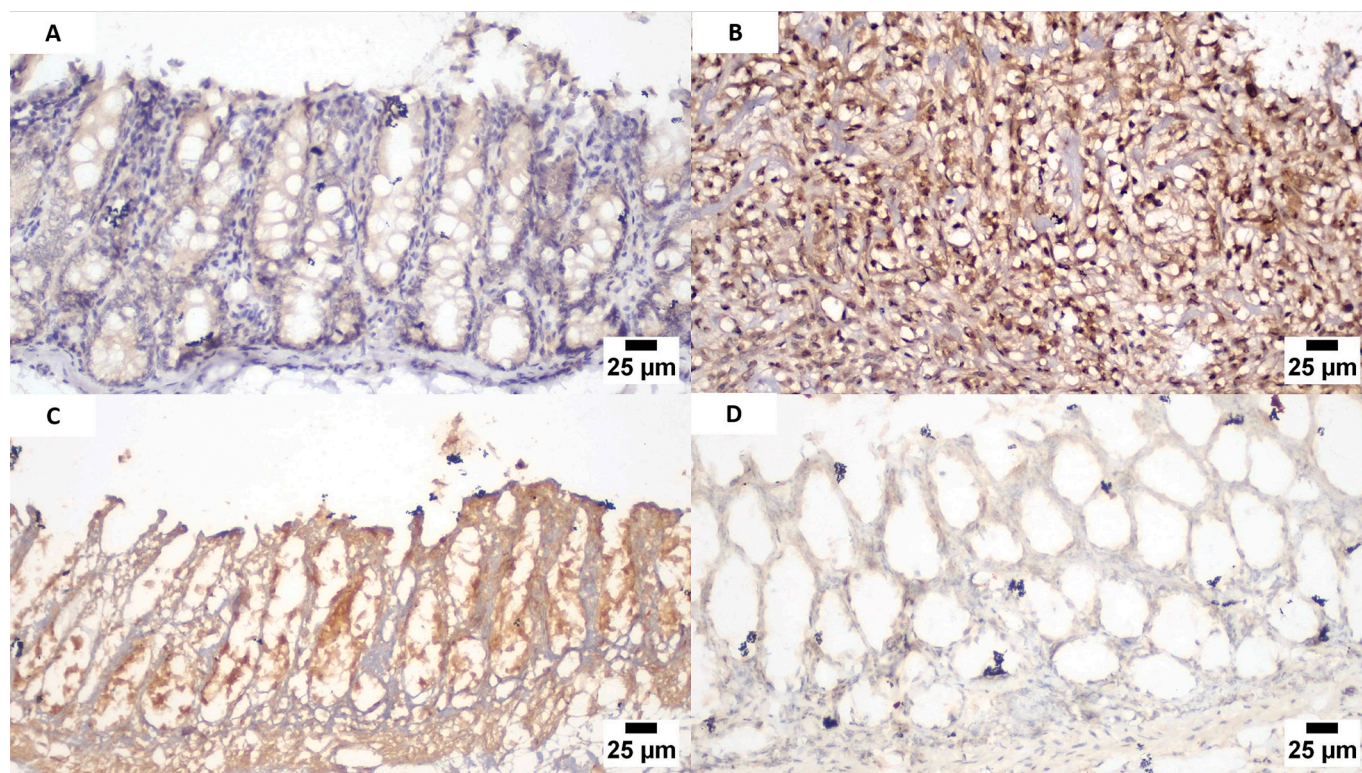
Fig. 8. Imunopathological features of normal control group (A) showed no reactivity to CXCR4 in colon mucosa and wall; DMH group (B) showed strong reactivity towards CXCR 4 in colon mucosal cells and colon wall; CLX- suspension (C) showed moderate colon mucosa and colon wall reactivity for CXCR 4; CLX-PEI-UENVs (D) showed a very mild to limited expression of CXCR4 in colon wall.

cancer mice model. Moreover, CXCR7 was reported to alter the CXCL12 receptor that aided in tumor rabid transcription and metastasis (Katoh et al., 2010). Additionally, CXCR7 induced damage of CXCR4 provoking its inability to activate G proteins after CXCL12 binding (Xu et al., 2023). Recently, Kassassir et al. (2023) stated that upregulation of CXCR4 is linked to cancer severity and survival. Bao et al. (2013) confirmed that the CXCL12/CXCR4 axis was involved in numerous pathways related to carcinogenesis and played a crucial role in tumor development, survival, angiogenesis, metastasis, and resistance to treatment. Thus, our colon section results of CXCR4 chemokines together with COX-2 inhibition via CLX-targeted nanoplatform could be employed as a successful therapeutic drug delivery approach to tackle CRC.

3.5.5. Histopathological examination

Microscopic examination of colon tissue samples from the normal colon section group revealed a normal structure that encompassed inner tunica mucosa containing glands with various mucus secreting cells and muscle in the outer layers, Fig. 9A.

Contrarily, DMH group sections exhibited marked histopathological alterations; represented by a complete mucosal destruction with an intensive inflammatory reaction in all layers with presence of neutrophils. Also, the glands displayed cystic dilatation with dysplastic alteration and a discernible decrease in goblet cells coupled with glandular epithelium exhibited hyperchromacia, anisokaryosis and frequent mitosis, Fig. 9B. Fleming et al. (2012) characterized a metastatic colorectal histopathological model that indicates cystic dilatation with dysplastic changes coupled with neutrophils presence. Such outcomes coincide with Eisa et al. (2022) who reported the same pathological changes presented in our data results.

On the other hand, treated CLX suspension colon sections revealed moderate improvement. Most of the examined sections exhibited intact lamina epithelialis and propria with inflammatory edema occupying the submucosa; while other sections showed mononuclear inflammatory cells infiltration at the propria with goblet cells hyperplasia and hyperactivity and other few sections showed complete destruction of the colonic wall with complete necrosis of mucosa and intense inflammatory cells infiltration, Fig. 9C. CLX-ES-PEI-UENVs exhibited better healing wherein part of the inspected sections disclosed obviously normal mucosa with slight mononuclear inflammatory cells infiltration, Fig. 9D. Recent research revealed that the histopathological mucosal damage has been healed upon treatment with CLX (Chen et al., 2023).

4. Conclusions

pH-triggered surface charge reversal nanovesicles, loaded with CLX, were successfully formulated to target the colorectal regions and augment the oral bioavailability of CLX. The formulated CLX-ES-PEI-UENVs exhibited high stability. CLX-UENVs and CLX-PEI-UENVs exhibited undesirable CLX release in a medium simulating the stomach and upper GIT pH. Nevertheless, the surface modification of CLX-PEI-UENVs with ES offered adequate protection for CLX in an acidic milieu and enhanced CLX release in a medium simulating the pH of the colorectal regions. Consequently, the enhanced accumulation of CLX in the target segments was facilitated by pH-induced charge reversal of CLX-ES-PEI-UENVs. Moreover, oral administration of CLX-ES-PEI-UENVs exhibited augmented bioavailability compared to CLX suspension. In experimental rats, the tested CLX-ES-PEI-UENVs shielded against CRC induced by DMH and proved superior activity over conventional CLX suspension. The apparent molecular mechanism behind this protection was via upregulation of Wnt/β-catenin pathway as well as downregulation of LEF 1/TCF 3 gene expression and inflammatory markers. Thus, the crafted CLX-ES-PEI-UENVs could confer a promising
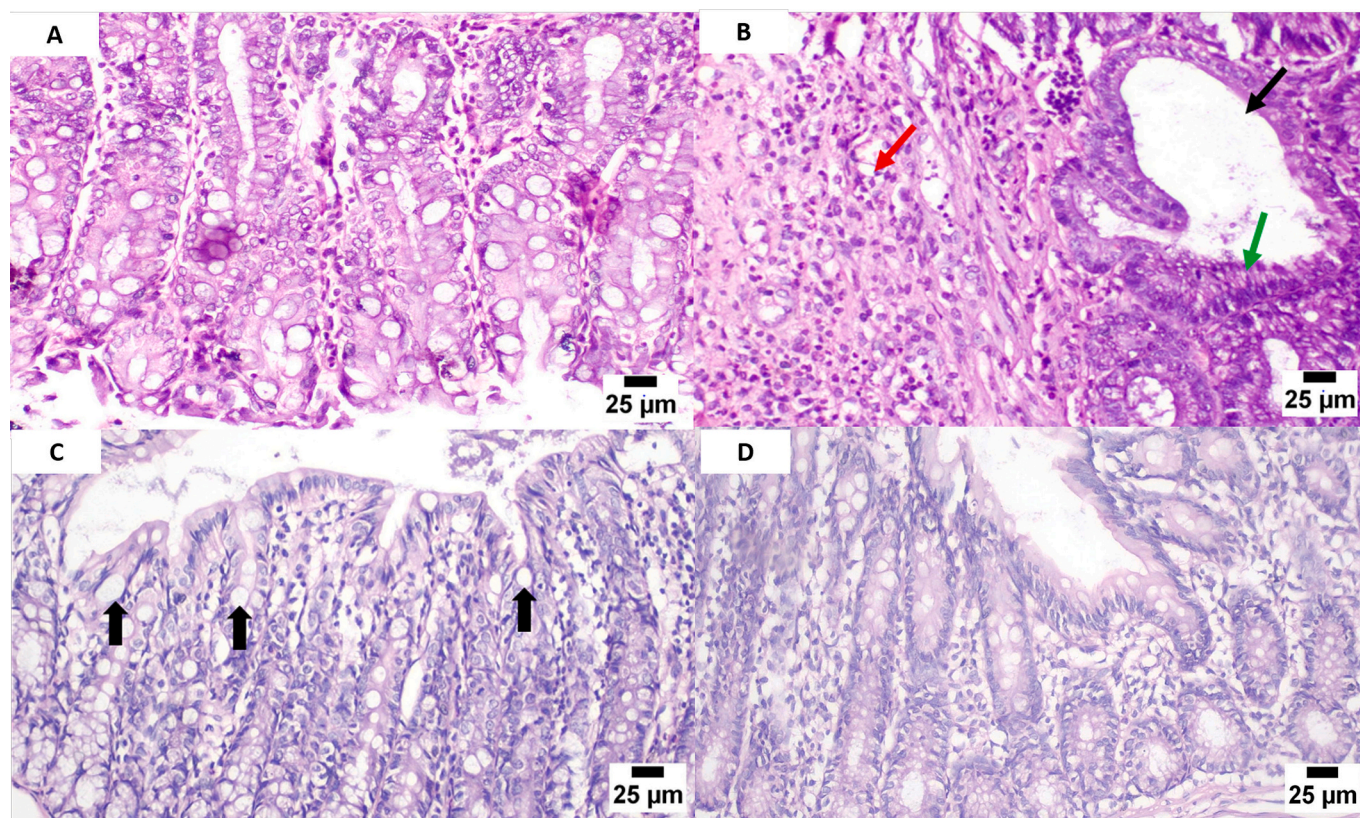
Fig. 9. Photomicrograph (H&E) of colon represents normal control section (A) with higher magnification showed normal structure of colon glands with numerous goblet cells; DMH group (B) showed cystically dilated gland (black arrow) with heavy inflammatory cells infiltration (red arrow), note the marked dysplasia in the glandular epithelium (green arrow); CLX suspension (C) showed hyperplasia and hyperactivity of mucous glands (arrows); CLX-PEI-UENVs (D) showed apparently normal propria with mild mononuclear inflammatory cells infiltration. (For interpretation of the references to colour in this figure legend, the reader is referred to the web version of this article.)

and tolerable nanoparadigm for CLX colorectal targeting which could overwhelm its oral-related obstacles meanwhile accomplishing clinical benefits for CRC management.

CRediT authorship contribution statement

Shahira F. El Menshawe: Writing – review & editing, Visualization, Validation, Supervision, Investigation, Conceptualization. **Khaled Shalaby:** Writing – review & editing, Validation, Supervision, Resources, Project administration. **Mohammed H. Elkomy:** Writing – review & editing, Writing – original draft, Visualization, Validation, Resources, Investigation, Conceptualization. **Heba M. Aboud:** Writing – review & editing, Writing – original draft, Visualization, Validation, Supervision, Software, Resources, Project administration, Methodology, Investigation, Formal analysis, Data curation, Conceptualization. **Yasmin M. Ahmed:** Writing – review & editing, Writing – original draft, Visualization, Validation, Supervision, Software, Resources, Project administration, Methodology, Investigation, Formal analysis, Data curation, Conceptualization. **Abdelmeged A. Abdelmeged:** Validation, Supervision, Investigation, Formal analysis, Conceptualization. **Marwa Elkarmalawy:** Writing – review & editing, Writing – original draft, Visualization, Validation, Investigation, Formal analysis, Conceptualization. **Mahmoud A. Abou Alazayem:** Writing – review & editing, Writing – original draft, Visualization, Validation, Software, Resources, Methodology, Investigation, Formal analysis, Data curation. **Amani M.**

El Sisi: Writing – review & editing, Writing – original draft, Visualization, Validation, Supervision, Software, Resources, Project administration, Methodology, Investigation, Formal analysis, Data curation, Conceptualization.

Declaration of Competing Interest

The authors wish to declare that no interest is involved in this publication.

Data availability

Data will be made available on request.

Appendix A. Supplementary data

Supplementary data to this article can be found online at https://doi.org/10.1016/j.ijpx.2023.100225.

References

Abdelbari, M.A., El-Mancy, S.S., Elshafeey, A.H., Abdelbary, A.A., 2021. Implementing spanlastics for improving the ocular delivery of clotrimazole: in vitro characterization, ex vivo permeability, microbiological assessment and in vivo safety study. Int. J. Nanomedicine 16, 6249.

Aboud, H.M., Hassan, A.H., Ali, A.A., Abdel-Razik, A.-R.H., 2018. Novel in situ gelling vaginal sponges of sildenafil citrate-based cubosomes for uterine targeting. Drug Deliv. 25, 1328–1339.

Aboud, H.M., Mahmoud, M.O., Abdeltawab Mohammed, M., Shafiq Awad, M., Sabry, D., 2020. Preparation and appraisal of self-assembled valsartan-loaded amalgamated Pluronic F127/Tween 80 polymeric micelles: boosted cardioprotection via regulation of Mhrt/Nrf2 and Trx1 pathways in cisplatin-induced cardiotoxicity. J. Drug Target. 28, 282–299.

Ahmad, A., Rehman, M.U., Wali, A.F., El-Serehy, H.A., Al-Misned, F.A., Maodaa, S.N., Aljawdah, H.M., Mir, T.M., Ahmad, P., 2020. Box–Behnken response surface design of polysaccharide extraction from rhododendron arboreum and the evaluation of its antioxidant potential. Molecules 25, 3835.

Albash, R., Abdelbary, A.A., Refai, H., El-Nabarawi, M.A., 2019. Use of transethosomes for enhancing the transdermal delivery of olmesartan medoxomil: in vitro, ex vivo, and in vivo evaluation. Int. J. Nanomedicine 14, 1953.

Al-Mahallawi, A.M., Khowessah, O.M., Shoukri, R.A., 2017. Enhanced non invasive trans-tympanic delivery of ciprofloxacin through encapsulation into nano-spanlastic vesicles: fabrication, in-vitro characterization, and comparative ex-vivo permeation studies. Int. J. Pharm. 522, 157–164.

Andersen, T., Vanić, Ž., Flaten, G.E., Mattsson, S., Tho, I., Škalko-Basnet, N., 2013. Pectosomes and chitosomes as delivery systems for metronidazole: the one-pot preparation method. Pharmaceutics 5, 445–456.

Anuja, K., Roy, S., Ghosh, C., Gupta, P., Bhattacharjee, S., Banerjee, B., 2017. Prolonged inflammatory microenvironment is crucial for pro-neoplastic growth and genome instability: a detailed review. Inflamm. Res. 66, 119–128.

Aoki, T., Nishida, N., Kudo, M., 2022. Clinical significance of the duality of Wnt/β-catenin signaling in human hepatocellular carcinoma. Cancers 14, 444.

Arber, N., Eagle, C.J., Spicak, J., Rácz, I., Dite, P., Hajer, J., Zavoral, M., Lechuga, M.J., Gerletti, P., Tang, J., 2006. Celecoxib for the prevention of colorectal adenomatous polyps. N. Engl. J. Med. 355, 885–895.

Assoni, G., La Pietra, V., Digilio, R., Ciani, C., Licata, N.V., Micaelli, M., Facen, E., Tomaszewska, W., Cerofolini, L., Perez-Rafols, A., 2022. HuR-targeted agents: an insight into medicinal chemistry, biophysical, computational studies and pharmacological effects on cancer models. Adv. Drug Deliv. Rev. 181, 114088.

Auman, J.T., Church, R., Lee, S.-Y., Watson, M.A., Fleshman, J.W., Mcleod, H.L., 2008. Celecoxib pre-treatment in human colorectal adenocarcinoma patients is associated with gene expression alterations suggestive of diminished cellular proliferation. Eur. J. Cancer 44, 1754–1760.

Aziz, D.E., Abdelbary, A.A., Elassasy, A.I., 2018. Implementing central composite design for developing transdermal diacerein-loaded niosomes: ex vivo permeation and in vivo deposition. Curr. Drug Deliv. 15, 1330–1342.

Babu, S.S.N., Singla, S., Jena, G., 2023. Role of combination treatment of aspirin and zinc in DMH-DSS-induced colon inflammation, oxidative stress and tumour progression in male BALB/c mice. Biol. Trace Elem. Res. 201, 1327–1343.

Bancroft, J.D., Gamble, M., 2008. Theory and Practice of Histological Techniques. Elsevier Health Sciences.

Bao, L., Lai, Y., Liu, Y., Qin, Y., Zhao, X., Lu, X., Jiang, Q., Lu, J., Huang, X., 2013. CXCR4 is a good survival prognostic indicator in multiple myeloma patients. Leuk. Res. 37, 1083–1088.

Basha, M., Abd El-Alim, S.H., Shamma, R.N., Awad, G.E., 2013. Design and optimization of surfactant-based nanovesicles for ocular delivery of Clotrimazole. J. Liposome Res. 23, 203–210.

Bazan, L., Bendas, E.R., El Gazayerly, O.N., Badawy, S.S., 2016. Comparative pharmaceutical study on colon targeted micro-particles of celecoxib: in-vitro–in-vivo evaluation. Drug Deliv. 23, 3339–3349.

Bijman, M.N., Hermelink, C.A., van Berkel, M.P., Laan, A.C., Janmaat, M.L., Peters, G.J., Boven, E., 2008. Interaction between celecoxib and docetaxel or cisplatin in human cell lines of ovarian cancer and colon cancer is independent of COX-2 expression levels. Biochem. Pharmacol. 75, 427–437.

Borowczak, J., Szczerbowski, K., Maniewski, M., Kowalewski, A., Janiczek-Polewska, M., Szylberg, A., Marszałek, A., Szylberg, Ł., 2022. The role of inflammatory cytokines in the pathogenesis of colorectal carcinoma—recent findings and review. Biomedicines 10, 1670.

Boztaş, N., Özbilgin, Ş., Özbilgin, M., Taylan, E., Ünlü, M., Özkardeşler, S., Akan, M., Yurtlu, V., Hancı, V., 2021. Effects of midazolam, propofol and thiopental on gastric ulcer in rats midazolam. Haydarpaşa Numune Med. J. 61, 24.

Buzzelli, J.N., Ouaret, D., Brown, G., Allen, P.D., Muschel, R.J., 2018. Colorectal cancer liver metastases organoids retain characteristics of original tumor and acquire chemotherapy resistance. Stem Cell Res. 27, 109–120.

Chen, R., Lin, X., Wang, Q., An, X., Zhao, X., Lin, Y., Sun, T., Yan, C., Cai, A., Cao, W., 2023. Dual-targeting celecoxib nanoparticles protect intestinal epithelium and regulate macrophage polarization for ulcerative colitis treatment. Chem. Eng. J. 452, 139445.

Danaei, M., Dehghankhold, M., Ataei, S., Hasanzadeh Davarani, F., Javanmard, R., Dokhani, A., Khorasani, S., Mozafari, M., 2018. Impact of particle size and polydispersity index on the clinical applications of lipidic nanocarrier systems. Pharmaceutics 10, 57.

Devaraj, G.N., Parakh, S., Devraj, R., Apte, S., Rao, B.R., Rambhau, D., 2002. Release studies on niosomes containing fatty alcohols as bilayer stabilizers instead of cholesterol. J. Colloid Interface Sci. 251, 360–365.

Eid, H.M., Elkomy, M.H., El Menshawe, S.F., Salem, H.F., 2019. Transfersomal nanovesicles for nose-to-brain delivery of ofloxacin for better management of bacterial meningitis: formulation, optimization by Box-Behnken design, characterization and in vivo pharmacokinetic study. J. Drug Deliv. Sci. Technol. 54, 101304.

Eid, H.M., Naguib, I.A., Alsantali, R.I., Alsalahat, I., Hegazy, A.M., 2021. Novel chitosan-coated niosomal formulation for improved management of bacterial conjunctivitis: a highly permeable and efficient ocular nanocarrier for azithromycin. J. Pharm. Sci. 110, 3027–3036.

Eisa, N.H., Said, E., Khodir, A.E., Sabry, D., Ebrahim, H.A., Elsherbini, D.M.A., Altemani, R., Alnasser, D.M., Elsherbiny, N.M., El-Sherbiny, M., 2022. Effect of diacerein on HOTAIR/IL-6/STAT3, Wnt/β-catenin and TLR-4/NF-κB/TNF-α axes in colon carcinogenesis. Environ. Toxicol. Pharmacol. 95, 103943.

Eissa, E.M., Elkomy, M.H., Eid, H.M., Ali, A.A., Abourehab, M.A., Alsubaiyel, A.M., Naguib, I.A., Alsalahat, I., Hassan, A.H., 2022. Intranasal delivery of granisetron to the brain via nanostructured cubosomes-based in situ gel for improved management of chemotherapy-induced emesis. Pharmaceutics 14, 1374.

El Menshawe, S.F., Nafady, M.M., Aboud, H.M., Kharshoum, R.M., Elkelawy, A.M.M.H., Hamad, D.S., 2019. Transdermal delivery of fluvastatin sodium via tailored spanlastic nanovesicles: mitigated Freund's adjuvant-induced rheumatoid arthritis in rats through suppressing p38 MAPK signaling pathway. Drug Deliv. 26, 1140–1154.

Elkomy, M.H., Alruwaili, N.K., Elmowafy, M., Shalaby, K., Zafar, A., Ahmad, N., Alsalahat, I., Ghoneim, M.M., Eissa, E.M., Eid, H.M., 2022a. Surface-modified bilosomes nanogel bearing a natural plant alkaloid for safe management of rheumatoid arthritis inflammation. Pharmaceutics 14, 563.

Elkomy, M.H., Eid, H.M., Elmowafy, M., Shalaby, K., Zafar, A., Abdelgawad, M.A., Rateb, M.E., Ali, M.R., Alsalahat, I., Abou-Taleb, H.A., 2022b. Bilosomes as a promising nanoplatform for oral delivery of an alkaloid nutraceutical: improved pharmacokinetic profile and snowballed hypoglycemic effect in diabetic rats. Drug Deliv. 29, 2694–2704.

El-Say, K.M., Abd-Allah, F.I., Lila, A.E., Hassan, A.E.-S.A., Kassem, A.E.A., 2016. Diacerein niosomal gel for topical delivery: development, in vitro and in vivo assessment. J. Liposome Res. 26, 57–68.

Elsherif, N.I., Shamma, R.N., Abdelbary, G., 2017. Terbinafine hydrochloride trans-ungual delivery via nanovesicular systems: in vitro characterization and ex vivo evaluation. AAPS PharmSciTech 18, 551–562.

Ferreira, J.C., Reis, M.B., Coelho, G.D., Gastaldello, G.H., Peti, A.P.F., Rodrigues, D.M., Bastos, J.K., Campo, V.L., Sorgi, C.A., Faccioli, L.H., 2021. Baccharin and p-coumaric acid from green propolis mitigate inflammation by modulating the production of cytokines and eicosanoids. J. Ethnopharmacol. 278, 114255.

Flanagan, D.J., Phesse, T.J., Barker, N., Schwab, R.H., Amin, N., Malaterre, J., Stange, D. E., Nowell, C.J., Currie, S.A., Saw, J.T., 2015. Frizzled7 functions as a Wnt receptor in intestinal epithelial Lgr5+ stem cells. Stem Cell Rep. 4, 759–767.

Fleming, M., Ravula, S., Tatishchev, S.F., Wang, H.L., 2012. Colorectal carcinoma: pathologic aspects. J. Gastrointest. Oncol. 3, 153.

Gehrke, I., Gandhirajan, R.K., Kreuzer, K.-A., 2009. Targeting the WNT/β-catenin/TCF/LEF1 axis in solid and haematological cancers: multiplicity of therapeutic options. Eur. J. Cancer 45, 2759–2767.

Hatem, E., Azzi, S., El Banna, N., He, T., Heneman-Masurel, A., Vernis, L., Baïlle, D., Masson, V., Dingli, F., Loew, D., 2019. Auranofin/vitamin C: a novel drug combination targeting triple-negative breast cancer. JNCI J. Natl. Cancer Inst. 111, 597–608.

He, M., Zhao, Z., Yin, L., Tang, C., Yin, C., 2009. Hyaluronic acid coated poly (butyl cyanoacrylate) nanoparticles as anticancer drug carriers. Int. J. Pharm. 373, 165–173.

Hiremath, P.S., Soppimath, K.S., Betageri, G.V., 2009. Proliposomes of exemestane for improved oral delivery: formulation and in vitro evaluation using PAMPA, Caco-2 and rat intestine. Int. J. Pharm. 380, 96–104.

Hiremath, I.S., Goel, A., Warrier, S., Kumar, A.P., Sethi, G., Garg, M., 2022. The multidimensional role of the Wnt/β-catenin signaling pathway in human malignancies. J. Cell. Physiol. 237, 199–238.

Hsiao, P.-W., Chang, C.-C., Liu, H.-F., Tsai, C.-M., Chiu, T.H., Chao, J.-I., 2007. Activation of p38 mitogen-activated protein kinase by celecoxib oppositely regulates survivin and gamma-H2AX in human colorectal cancer cells. Toxicol. Appl. Pharmacol. 222, 97–104.

Hu, J., Su, X.-J., Si, H.-L., Song, R.-X., Zhang, F., Qiu, X.-J., Chen, X.-P., 2021. Simultaneous determination of celecoxib, dezocine and dexmedetomidine in beagle plasma using UPLC-MS/MS method and the application in pharmacokinetics. Drug Des. Devel. Ther. 15, 2529.

Huang, L., Zhang, J., Deng, Y., Wang, H., Zhao, P., Zhao, G., Zeng, W., Wang, Y., Chen, C., Wagstaff, W., 2023. Niclosamide (NA) Overcomes Cisplatin Resistance in Human Ovarian cancer. Genes & Diseases.

Ibrahim, N., Raman, I., Yusop, M.R., 2015. Effects of functional group of non-ionic surfactants on the stability of emulsion. Malays. J. Anal. Sci. 19, 261–267.

Kaiser, A., Eiselt, G., Bechler, J., Huber, O., Schmidt, M., 2023. WNT3a signaling inhibits aromatase expression in breast adipose fibroblasts—a possible mechanism supporting the loss of estrogen responsiveness of triple-negative breast cancers. Int. J. Mol. Sci. 24, 4654.

Kassassir, H., Papiewska-Pająk, I., Kryczka, J., Boncela, J., Kowalska, M.A., 2023. Platelet-derived microparticles stimulate the invasiveness of colorectal cancer cells via the p38MAPK-MMP-2/MMP-9 axis. Cell Commun. Signal. 21, 1–13.

Katoh, H., Hosono, K., Ito, Y., Suzuki, T., Ogawa, Y., Kubo, H., Kamata, H., Mishima, T., Tamaki, H., Sakagami, H., 2010. COX-2 and prostaglandin EP3/EP4 signaling regulate the tumor stromal proangiogenic microenvironment via CXCL12-CXCR4 chemokine systems. Am. J. Pathol. 176, 1469–1483.

Kendall, R.A., Alhnan, M.A., Nilkumhang, S., Murdan, S., Basit, A.W., 2009. Fabrication and in vivo evaluation of highly pH-responsive acrylic microparticles for targeted gastrointestinal delivery. Eur. J. Pharm. Sci. 37, 284–290.

Khallaf, R.A., Aboud, H.M., Sayed, O.M., 2020. Surface modified niosomes of olanzapine for brain targeting via nasal route; preparation, optimization, and in vivo evaluation. J. Liposome Res. 30, 163–173.

Kim, J.-Y., Song, M.-G., Kim, J.-D., 2000. Zeta potential of nanobubbles generated by ultrasonication in aqueous alkyl polyglycoside solutions. J. Colloid Interface Sci. 223, 285–291.

Kim, J., Mori, T., Chen, S.L., Amersi, F.F., Martinez, S.R., Kuo, C., Turner, R.R., Ye, X., Bilchik, A.J., Morton, D.L., 2006. Chemokine receptor CXCR4 expression in patients with melanoma and colorectal cancer liver metastases and the association with disease outcome. Ann. Surg. 244, 113.

Kolluri, A., Ho, M., 2019. The role of glypican-3 in regulating Wnt, YAP, and hedgehog in liver cancer. Front. Oncol. 9, 708.

Kundu, J., Chung, Y.-I., Kim, Y.H., Tae, G., Kundu, S., 2010. Silk fibroin nanoparticles for cellular uptake and control release. Int. J. Pharm. 388, 242–250.

Kuwai, T., Nakamura, T., Sasaki, T., Kitadai, Y., Kim, J.-S., Langley, R.R., Fan, D., Wang, X., Do, K.-A., Kim, S.-J., 2008. Targeting the EGFR, VEGFR, and PDGFR on colon cancer cells and stromal cells is required for therapy. Clin. Exp. Metastasis 25, 477–489.

Lee, D.-Y., Song, M.-Y., Kim, E.-H., 2021. Role of oxidative stress and Nrf2/KEAP1 signaling in colorectal cancer: mechanisms and therapeutic perspectives with phytochemicals. Antioxidants 10, 743.

Lequin, R.M., 2005. Enzyme immunoassay (EIA)/enzyme-linked immunosorbent assay (ELISA). Clin. Chem. 51, 2415–2418.

Lin, S., Zhen, Y., Guan, Y., Yi, H., 2020. Roles of wnt/β-catenin signaling pathway regulatory long non-coding RNAs in the pathogenesis of non-small cell lung cancer. Cancer Manag. Res. 12, 4181.

Liu, C.-F., Samsa, W.E., Zhou, G., Lefebvre, V., 2017. Transcriptional control of chondrocyte specification and differentiation. In: Seminars in Cell & Developmental Biology. Elsevier, pp. 34–49.

Livak, K.J., Schmittgen, T.D., 2001. Analysis of relative gene expression data using real-time quantitative PCR and the $2-\Delta\Delta CT$ method. Methods 25, 402–408.

Locke, J., Da Silva Xavier, G., Rutter, G., Harries, L., 2011. An alternative polyadenylation signal in TCF7L2 generates isoforms that inhibit T cell factor/lymphoid-enhancer factor (TCF/LEF)-dependent target genes. Diabetologia 54, 3078–3082.

Lu, Y., Li, J., Wang, G., 2008. In vitro and in vivo evaluation of mPEG-PLA modified liposomes loaded glycyrrhetinic acid. Int. J. Pharm. 356, 274–281.

Mahmoud, M.O., Aboud, H.M., Hassan, A.H., Ali, A.A., Johnston, T.P., 2017. Transdermal delivery of atorvastatin calcium from novel nanovesicular systems using polyethylene glycol fatty acid esters: ameliorated effect without liver toxicity in poloxamer 407-induced hyperlipidemic rats. J. Control. Release 254, 10–22.

Mandal, B.B., Kundu, S., 2009. Self-assembled silk sericin/poloxamer nanoparticles as nanocarriers of hydrophobic and hydrophilic drugs for targeted delivery. Nanotechnology 20, 355101.

Merz, H., Malisius, R., Mannweiler, S., Zhou, R., Hartmann, W., Orscheschek, K., Moubayed, P., Feller, A., 1995. ImmunoMax. A maximized immunohistochemical method for the retrieval and enhancement of hidden antigens. Lab. Investig. 73, 149–156.

Monteleone, N.J., Lutz, C.S., 2021. miR-708 negatively regulates TNFα/IL-1β signaling by suppressing NF-κB and arachidonic acid pathways. Mediat. Inflamm. 2021.

Naeem, M., Oshi, M.A., Kim, J., Lee, J., Cao, J., Nurhasni, H., Im, E., Jung, Y., Yoo, J.-W., 2018. pH-triggered surface charge-reversal nanoparticles alleviate experimental murine colitis via selective accumulation in inflamed colon regions. Nanomedicine 14, 823–834.

Nakamura, Y., Mochida, A., Choyke, P.L., Kobayashi, H., 2016. Nanodrug delivery: is the enhanced permeability and retention effect sufficient for curing cancer? Bioconjug. Chem. 27, 2225–2238.

Nascimento-Gonçalves, E., Mendes, B.A., Silva-Reis, R., Faustino-Rocha, A.I., Gama, A., Oliveira, P.A., 2021. Animal models of colorectal cancer: from spontaneous to genetically engineered models and their applications. Vet. Sci. 8, 59.

Niebel, W., Walkenbach, K., Béduneau, A., Pellequer, Y., Lamprecht, A., 2012. Nanoparticle-based clodronate delivery mitigates murine experimental colitis. J. Control. Release 160, 659–665.

Nigam, M., Mishra, A.P., Deb, V.K., Dimri, D.B., Tiwari, V., Bungau, S.G., Bungau, A.F., Radu, A.-F., 2023. Evaluation of the association of chronic inflammation and cancer: insights and implications. Biomed. Pharmacother. 164, 115015.

Panda, D.S., Eid, H.M., Elkomy, M.H., Khames, A., Hassan, R.M., Abo El-Ela, F.I., Yassin, H.A., 2021. Berberine encapsulated Lecithin–Chitosan nanoparticles as innovative wound healing agent in type II diabetes. Pharmaceutics 13, 1197.

Paulson, S.K., Zhang, J.Y., Breau, A.P., Hribar, J.D., Liu, N.W., Jessen, S.M., Lawal, Y.M., Cogburn, J.N., Gresk, C.J., Markos, C.S., 2000. Pharmacokinetics, tissue distribution, metabolism, and excretion of celecoxib in rats. Drug Metab. Dispos. 28, 514–521.

Peschel, N., Wright, J.T., Koster, M.I., Clarke, A.J., Tadini, G., Fete, M., Hadj-Rabia, S., Sybert, V.P., Norderyd, J., Maier-Wohlfart, S., 2022. Molecular pathway-based classification of ectodermal dysplasias: first five-yearly update. Genes 13, 2327.

Pushpakom, S., Iorio, F., Eyers, P.A., Escott, K.J., Hopper, S., Wells, A., Doig, A., Guilliams, T., Latimer, J., McNamee, C., 2019. Drug repurposing: progress, challenges and recommendations. Nat. Rev. Drug Discov. 18, 41–58.

Qu, G., Yao, Z., Zhang, C., Wu, X., Ping, Q., 2009. PEG conjugated N-octyl-O-sulfate chitosan micelles for delivery of paclitaxel: in vitro characterization and in vivo evaluation. Eur. J. Pharm. Sci. 37, 98–105.

Sadighparvar, S., Darband, S.G., Yousefi, B., Kaviani, M., Ghaderi-Pakdel, F., Mihanfar, A., Babaei, G., Mobaraki, K., Majidinia, M., 2020. Combination of quercetin and exercise training attenuates depression in rats with 1, 2-dimethylhy-drazine-induced colorectal cancer: possible involvement of inflammation and BDNF signalling. Exp. Physiol. 105, 1598–1609.

Salem, H.F., Ali, A.A., Hegazy, A.M., Sadek, A.-R.A., Aboud, H.M., 2022. Harnessing of doxylamine succinate/pyridoxine hydrochloride-dual laden bilosomes as a novel combinatorial nanoparadigm for intranasal delivery: in vitro optimization and in vivo pharmacokinetic appraisal. J. Pharm. Sci. 111, 794–809.

Samadarsi, R., Augustin, L., Kumar, C., Dutta, D., 2022. In-silico and in-vitro studies on the efficacy of mangiferin against colorectal cancer. BMC Chem. 16, 42.

Sasaki, T., Kitadai, Y., Nakamura, T., Kim, J.-S., Tsan, R.Z., Kuwai, T., Langley, R.R., Fan, D., Kim, S.-J., Fidler, I.J., 2007. Inhibition of epidermal growth factor receptor and vascular endothelial growth factor receptor phosphorylation on tumor-associated endothelial cells leads to treatment of orthotopic human colon cancer in nude mice. Neoplasia 9, 1066–1077.

Schneider, J.A., Logan, S.K., 2018. Revisiting the role of Wnt/β-catenin signaling in prostate cancer. Mol. Cell. Endocrinol. 462, 3–8.

Sobolewski, C., Cerella, C., Dicato, M., Ghibelli, L., Diederich, M., 2010. The role of cyclooxygenase-2 in cell proliferation and cell death in human malignancies. Int. J. Cell Biol. 2010.

Srivastava, S., Dewangan, J., Mishra, S., Divakar, A., Chaturvedi, S., Wahajuddin, M., Kumar, S., Rath, S.K., 2021. Piperine and Celecoxib synergistically inhibit colon cancer cell proliferation via modulating Wnt/β-catenin signaling pathway. Phytomedicine 84, 153484.

Steinbach, G., Lynch, P.M., Phillips, R.K., Wallace, M.H., Hawk, E., Gordon, G.B., Wakabayashi, N., Saunders, B., Shen, Y., Fujimura, T., 2000. The effect of celecoxib, a cyclooxygenase-2 inhibitor, in familial adenomatous polyposis. N. Engl. J. Med. 342, 1946–1952.

Takamoto, I., Kubota, N., Nakaya, K., Kumagai, K., Hashimoto, S., Kubota, T., Inoue, M., Kajiwara, E., Katsuyama, H., Obata, A., 2014. TCF7L2 in mouse pancreatic beta cells plays a crucial role in glucose homeostasis by regulating beta cell mass. Diabetologia 57, 542–553.

Tayel, S.A., El-Nabarawi, M.A., Tadros, M.I., Abd-Elsalam, W.H., 2015. Duodenum-triggered delivery of pravastatin sodium via enteric surface-coated nanovesicular spanlastic dispersions: development, characterization and pharmacokinetic assessments. Int. J. Pharm. 483, 77–88.

Terry, S., Yang, X., Chen, M.W., Vacherot, F., Buttyan, R., 2006. Multifaceted interaction between the androgen and Wnt signaling pathways and the implication for prostate cancer. J. Cell. Biochem. 99, 402–410.

Tewari, D., Bawari, S., Sharma, S., DeLiberto, L.K., Bishayee, A., 2021. Targeting the crosstalk between canonical Wnt/β-catenin and inflammatory signaling cascades: a novel strategy for cancer prevention and therapy. Pharmacol. Ther. 227, 107876.

Vandamme, T.F., Lenourry, A., Charrueau, C., Chaumeil, J., 2002. The use of polysaccharides to target drugs to the colon. Carbohydr. Polym. 48, 219–231.

Venkatesan, P., Puvvada, N., Dash, R., Kumar, B.P., Sarkar, D., Azab, B., Pathak, A., Kundu, S.C., Fisher, P.B., Mandal, M., 2011. The potential of celecoxib-loaded hydroxyapatite-chitosan nanocomposite for the treatment of colon cancer. Biomaterials 32, 3794–3806.

Wacker, M., 2013. Nanocarriers for intravenous injection—the long hard road to the market. Int. J. Pharm. 457, 50–62.

Wang, D., DuBois, R.N., 2006. Prostaglandins and cancer. Gut 55, 115–122.

Wang, S.-C., Lin, J.-K., Wang, H.-S., Yang, S.-H., Li, A.F.-Y., Chang, S.-C., 2010. Nuclear expression of CXCR4 is associated with advanced colorectal cancer. Int. J. Color. Dis. 25, 1185–1191.

Wang, M., Li, J., Wang, D., Xin, Y., Liu, Z., 2023. The effects of mesenchymal stem cells on the chemotherapy of colorectal cancer. Biomed. Pharmacother. 160, 114373.

Xia, J., Pei, L., Zhuang, J., Ji, Y., Xu, G., Zhang, Z., Li, N., Yan, J., 2010. Celecoxib inhibits β-catenin-dependent survival of the human osteosarcoma MG-63 cell line. J. Int. Med. Res. 38, 1294–1304.

Xu, J., Yang, F., Luo, S., Gao, Y., Huang, D., Zhang, L., 2023. The role of SDF-1α-CXCR4/CXCR7 in migration of human periodontal ligament stem cells. Int. J. Stem Cells 16, 180–190.

Yuan, X., Xue, J., Tan, Y., Yang, Q., Qin, Z., Bao, X., Li, S., Pan, L., Jiang, Z., Wang, Y., 2021. Albuca bracteate polysaccharides synergistically enhance the anti-tumor efficacy of 5-fluorouracil against colorectal cancer by modulating β-catenin signaling and intestinal flora. Front. Pharmacol. 12, 736627.

Zhang, X., Yan, K., Deng, L., Liang, J., Liang, H., Feng, D., Ling, B., 2019. Cyclooxygenase 2 promotes proliferation and invasion in ovarian cancer cells via the PGE2/NF-κB pathway. Cell Transplant. 28, 1S–13S.

Zhao, H., Wu, L., Yan, G., Chen, Y., Zhou, M., Wu, Y., Li, Y., 2021. Inflammation and tumor progression: signaling pathways and targeted intervention. Signal Transduct. Target. Ther. 6, 263.

Zhao, H., Ming, T., Tang, S., Ren, S., Yang, H., Liu, M., Tao, Q., Xu, H., 2022. Wnt signaling in colorectal cancer: pathogenic role and therapeutic target. Mol. Cancer 21, 144.

Zhou, H., Lin, C., Zhang, Y., Zhang, X., Zhang, C., Zhang, P., Xie, X., Ren, Z., 2017. miR-506 enhances the sensitivity of human colorectal cancer cells to oxaliplatin by suppressing MDR 1/P-gp expression. Cell Prolif. 50, e12341.